N-acetylcarnosine attenuates age-associated declines in multi-organ systems to improve survival

Edwin R. Miranda[1,2,3], Justin L. Shahtout[1,3,4], Shinya Watanabe[1,3], Jan Spaas[5], Norah Y. Milam[1,3], Grace Neiswanger[1,3], Benjamin Werbner[1,2,3], Deborah Stuart[6], Sohom Mookherjee[1,3], Jack Wilson[1], Michael Judge[1], Isabella Y. Goh[7], Tyler Slater[8], Molly R. Gallop[1,2,3], Guoli Hu[9], Takuya Karasawa[1,2,3], Jillian K. Landers[1,3], Bryann Rainbow[1,3], Kyle T. O'Connor[10], Nicholas J. Black[10], He Lan[10], Linda S. Nikolova[11], Ying Li[1,3,12], Crystal F. Davey[1,10,13], James E. Cox [3,12,14], Sihem Boudina[1,2,3,15], Courtney M. Karner[9,16], Natalia S. Harasymowicz[2,7], Nirupama Ramkumar[3,6], J. David Symons[1,2,3,16], Amandine Chaix[1,2,3], Jonathan Z. Long[5], Micah J. Drummond[1,2,3,4,15], Katsuhiko Funai[1,2,3,4,14,15].

Affiliations

[1]Department of Nutrition and Integrative Physiology, University of Utah, Salt Lake City, Utah, United States.

[2]Molecular Medicine Program, University of Utah, Salt Lake City, Utah, United States.

[3]Diabetes & Metabolism Research Center, University of Utah, Salt Lake City, Utah, United States.

[4]Department of Physical Therapy & Athletic Training, University of Utah, Salt Lake City, Utah, United States.

[5]Department of Pathology, Stanford University, Stanford, California, United States.

[6]Division of Nephrology, Department of Internal Medicine, University of Utah, Salt Lake City, Utah, United States.

[7]Department of Orthopaedic Surgery Operations, University of Utah, Salt Lake City, Utah, United States.

[8]Preclinical Imaging Core Facility, University of Utah, Salt Lake City, Utah, United States.

[9]Department of Internal Medicine, University of Texas Southwestern, Dallas, Texas, United States.

[10]Transgenic Mouse Core Facility, University of Utah, Salt Lake City, Utah, United States.

[11]Electron Microscopy Facility, University of Utah, Salt Lake City, Utah, United States.

[12]Metabolomics Core Research Facility, University of Utah, Salt Lake City, United States.

[13]Mutation Generation & Detection Core Facility, University of Utah, Salt Lake City, United States.

[14]Department of Biochemistry, University of Utah School of Medicine, Salt Lake City, United States.

[15]Center on Aging, University of Utah, Salt Lake City, Utah, United States.

[16]Charles and Jane Pak Center for Mineral Metabolism and Clinical Research, University of Texas Southwestern, Dallas, Texas, United States.

Corresponding Author:

Katsuhiko Funai

University of Utah

15N, 2030E, Salt Lake City, UT 84112, USA

Email: kfunai@health.utah.edu

Abstract

Histidine containing dipeptides (HCDs) such as N-acetylcarnosine are endogenous metabolites that are ergogenic and mitigate metabolic dysfunction. We previously demonstrated that short-term N-acetylcarnosine treatment is highly efficacious in protecting muscle atrophy induced by disuse. Here we demonstrate that a 6-months treatment of N-acetylcarnosine attenuates a broad spectrum of age-associated maladies and improved survival by ~50% in female mice. A comprehensive survey of organ systems revealed that N-acetylcarnosine prevents decline in adiposity, diastolic function, vasodilation, muscle strength, and bone density. Together, N-acetylcarnosine substantially delays the onset of system-wide end-stage pathology to prolong lifespan. As an endogenously present metabolite, treatment with N-acetylcarnosine may be a safe and promising intervention to promote healthy aging in humans.

Introduction

With the aging global population, there remains an unmet need for therapies to mitigate age-related pathologies. While lifestyle modifications such as caloric restriction[1,2] and exercise[3] are effective strategies for prolonging health during aging, no equivocal pharmacologic strategies exist. Histidine containing dipeptides (HCDs) are endogenously produced metabolites primarily in excitable tissues[4] such as skeletal and cardiac muscle by conjugating histidine with beta-alanine or gamma-aminobutyric acid (GABA) in the case of homocarnosine. The supplementation of β-alanine, which is the rate limiting metabolite for HCD production, is ergogenic in humans, improving aerobic performance and muscle force production[5]. Conversely, decline in the HCD N-acetylcarnosine predicts mental and physical frailty in octogenarians[6]. The purported primary mechanism for these health benefits involves the scavenging of reactive carbonyl species, especially lipid-derived carbonyls such as 4-hydroxynonenal (4HNE) via the imidazole ring of histidine[7]. 4HNE and other reactive carbonyl species are generated via oxidation of their metabolic precursors. For example, 4HNE is produced primarily via peroxidation of ω6-polyunsaturated lipids. Formation of reactive carbonyls are accelerated in contexts of oxidative stress such as aging[8]. These reactive carbonyls non-enzymatically and irreversibly bind to proteins on nucleophilic residues incurring consequences such as impaired protein structure, function, and turnover[9,10].

HCD supplementation mitigates impairments in cardiovascular, musculoskeletal, neuronal and metabolic systems in contexts other than aging[11]. For example, supplementation with carnosine or its analog carnosinol improved glucose tolerance in mice and humans with obesity[12,13]. We recently demonstrated the ability of carnosine or N-acetylcarnosine supplementation to attenuate accumulation of 4HNE-modified proteins and preserve muscle mass and *ex vivo* force production in mice subjected to 7-days of inactivity[14]. Similarly, increasing muscle carnosine in older adults by supplementing with β-alanine improved muscle power and work capacity[15]. Nonetheless, there

82 has never been a study that examined the efficacy of long-term HCD supplementation on aging
83 *per se*. HCDs have excellent safety profiles with only mild side effects[13,15,16], making them
84 attractive to administer to humans over the course of aging. Herein, we performed a 6-month
85 preclinical N-acetylcarnosine trial in 18-24 months old mice and performed systematic
86 phenotyping of their organ systems to determine its effects on age-related health decline. We
87 chose N-acetylcarnosine primarily because we believed it would be more a translatable therapy
88 for humans due to its superior stability in human plasma compared to carnosine. Unlike mice,
89 humans ubiquitously express carnosinase (CN1) which hydrolyzes carnosine and other HCDs
90 limiting their stability in circulation. However, N-acetylcarnosine, which is largely unique to
91 humans, is not susceptible to CN1 hydrolysis.
92
93 C57Bl/6 mice from the aged rodent colony at the National Institute on Aging were acquired at 17
94 months of age. Following acclimation in our facility, the intervention was initiated at 18 months of
95 age and continued for 6 months. During the final month of the intervention, *in vivo* physiological
96 metrics spanning metabolic, neuro-endocrine, cardiovascular, renal, and musculoskeletal
97 systems were assessed. After the 6-month intervention, mice were anesthetized, and tissues
98 were collected for various assessments (Figure 1A).
99
100 **Results**
101 To confirm efficacy of our treatment, N-acetylcarnosine and other histidine-related metabolites
102 (Figure 1B) were quantified in various tissues. As anticipated[4], N-acetylcarnosine was only
103 appreciably quantifiable in tissues from N-acetylcarnosine-treated mice (Figure 1C, Supp. Figure
104 1). Given the role of N-acetylcarnosine to scavenge free carbonyls and prevent protein
105 carbonylation, we also measured protein carbonyls in these tissues. Consistent with this notion,
106 abundances for protein carbonyls were lower in several tissues from N-acetylcarnosine-treated
107 mice compared to vehicle-treated mice (Figure 1D, Supp. Figure 1). Carnosine, and the other

108 HCDs assayed were largely not enriched and some were even reduced by N-acetylcarnosine
109 treatment (Figure 1E-H, Supp. Figure 1). In skeletal muscle, heart, and gonadal white adipose
110 tissue (gWAT), N-acetylcarnosine enrichment was greater in female mice than in male mice. This
111 observation is in accord with many of the sex-specific effects we observed on physiologic
112 functions assayed.
113
114 At the 24-month timepoint, N-acetylcarnosine increased survival by ~50% only in female mice
115 (Figure 1I&J). In line with published female survival rates for this colony[17], approximately half of
116 the vehicle-treated female mice survived to approximately 24 months of age, while more than
117 75% of N-acetylcarnosine-treated female mice survived to this age. N-acetylcarnosine did not
118 influence survival in male mice by the end of the study (~24-month of age) (Figure 1J). It is
119 important to note that 75% survival for 24-month old male mice in this colony is in line with
120 published survival rates for male mice in this colony[17]. Concomitant with the increased survival,
121 N-acetylcarnosine promoted a retention of body weight that was also specific to female mice
122 (Figure 2A&B). The effect of N-acetylcarnosine on maintaining body weight was not explained by
123 differences in lean mass (Figure 2C&D) but instead was exclusively accounted for by its ability to
124 retain fat mass (Figure 2E&F). Importantly, these sex-specific effects were not explained by
125 differences in food consumption, or exposure to N-acetylcarnosine via water consumption (Supp.
126 Fig 2A-F).
127
128 Short-term N-acetylcarnosine or other HCDs may mitigate metabolic dysfunction associated with
129 obesity[12,18-22]. Consistent with the body composition data, N-acetylcarnosine treatment promoted
130 greater gWAT mass without influencing inguinal white adipose tissue (iWAT) or brown adipose
131 tissue BAT mass in female (Figure 2G&H) but not male (Supp. Figure 3A) mice. It's noteworthy
132 that N-acetylcarnosine was robustly enriched in gWAT only in female mice (and not in male mice)
133 whereas it was equally enriched in iWAT between sexes (Figure 1B, Supp. Figure 1). However,

134 protein carbonyls were equivocal in between groups in male and female mice (Figure 1C, Supp.
135 Figure 1). Similarly, liver, another metabolic organ influenced by adiposity, did not appear to be
136 affected in mass or histology by N-acetylcarnosine (Figure 2I&J, Supp. Figure 3A&B). Systemic
137 glucose tolerance was also not different between groups (Figure 3A, Supp. Figure 3C,D,K).
138
139 We further examined the effect of N-acetylcarnosine on systemic metabolism by Indirect
140 calorimetry. Surprisingly, whole-body O_2 consumption and energy expenditure were consistently
141 reduced in the N-acetylcarnosine treatment group in both sexes (Figure 3B, Supp. Figure 3E,F,L),
142 despite greater body weight in N-acetylcarnosine-treated female mice (Figure 2A). Respiratory
143 exchange ratio (RER), defined by CO_2 produced per O_2 consumed, is an indirect parameter to
144 estimate systemic substrate preference. An RER of 1.0 indicates exclusive glycolytic oxidation,
145 while a RER of 0.7 indicates exclusive fat oxidation. N-acetylcarnosine treatment did not have
146 any effect on RER in male mice (Supp. Figure 3H). Somewhat surprisingly, N-acetylcarnosine
147 treatment reduced RER in female mice (Figure 3C), normally a signature of improved metabolic
148 health[23]. These effects on metabolism are most likely explained by reduced ambulatory activity
149 that was observed in the female (Figure 3D, Supp. Fig 3M&N) but not male (Supp. Figure 3G,I,J)
150 N-acetylcarnosine-treated mice. Overall, N-acetylcarnosine preserved fat mass in female mice
151 without signs of metabolic dysfunction. In the context of aging, retention of adiposity represents
152 the ability of animals to maintain energy reserve which may delay frailty and promote longevity.
153
154 For male mice, we also assessed the effect of N-acetylcarnosine on fertility by assessing sperm
155 count and sperm viability. Sperm count decreases dramatically between 18 and 25 months in
156 C57Bl/6 mice[24] and the HCD carnosine is able to preserve sperm morphology in an accelerated
157 aging senescent mouse model[25]. However, N-acetylcarnosine did not affect sperm count, or the
158 percentage of live sperm in 24-month-old mice (Supp. Figure 4A).
159

160 Carnosine and other HCDs have also been implicated in improving neurologic function in aged
161 animal and human models[26-28]. Thus, we performed a wide variety of assessments to examine
162 the influence of N-acetylcarnosine treatment on the neurological system. N-acetylcarnosine
163 treatment did not have any effects on brain size in either sex (Figure 3E, Supp. Figure 4B). The
164 behavioral assessments also did not show differences in memory (fear conditioning and Y-maze)
165 (Figure 3F&G, Supp. Figure 4C,D,F) or pain perception (mechanical or heat)[29] (Figure 3H, Supp.
166 Figure 4E&G) in male or female mice.
167
168 As one of the organ systems critical for survival we next profiled the influence of N-acetylcarnosine
169 on cardio-renal phenotypes. N-acetylcarnosine treatment did not alter relative heart weight
170 (Figure 4A, Supp. Figure 5A) or histology (Figure 4B, Supp. Figure 5H). There was a modest
171 trend for lower heart rates in female mice (Figure 4C), suggesting a potentially positive effect of
172 N-acetylcarnosine on heart or perhaps vagal tone. Fractional shortening (FS) in female N-
173 acetylcarnosine-treated hearts was lower compared to the vehicle-treated mice (Figure 4F) with
174 no changes to cardiac output or ejection fraction (Figure 4D&E). The lower FS was driven by
175 ~17% greater systolic left ventricular internal diameter compared to vehicle mice (p=0.002, data
176 not shown), which suggests the N-acetylcarnosine treated mice are able to achieve similar blood
177 delivery as the vehicle-treated mice with less forceful systolic contraction. This could indicate that
178 the hearts from N-acetylcarnosine treated female mice have improved ventricular filling or are
179 pumping blood against a lower afterload (systemic blood pressure). Metrics of diastolic function
180 (E/A – indicative of filling velocity across the mitral anulus and E/e' – indicative of late-diastolic
181 ventricular filling) were not different in female mice (Figure 4G&H). Acetylcholine-evoked,
182 endothelium-dependent vasodilation assessed using isometric myography was similar in vehicle
183 and N-acetylcarnosine-treated mice (Figure 4I). However, addition of the endothelial nitric oxide
184 synthase (eNOS) inhibitor L-NMMA attenuated vasorelaxation to a greater extent in vessels from
185 N-acetylcarnosine compared to vehicle-treated mice (Figure 4I), a result that was substantiated

186 by arteries from N-acetylcarnosine mice displaying a greater calculated nitric oxide bioavailability
187 compared to vehicle mice (Figure 4J). Vascular smooth muscle responses were similar between
188 groups (not shown). These findings are consistent with previous work that HCDs promote
189 endothelium-dependent vasodilation[32,33], and might have implications concerning systemic blood
190 pressure.
191
192 N-acetylcarnosine appeared to influence heart to a lesser extent in male mice (Supp. Figure 5B-
193 F), except for improved E/e' indicative of late-diastolic ventricular filling (Supp. Figure 5G). It is
194 important to point out that the N-acetylcarnosine treatment in our study started when mice were
195 18-months old, an age when some of the age-related decline in heart function had already
196 began[30]. Thus, it remains possible that the treatment may have had a more substantial effect if
197 initiated earlier. This is particularly the case as HCDs have been shown to improve excitation-
198 contraction coupling via regulating calcium handling[31]. Overall, N-acetylcarnosine
199 supplementation may improve some aspects of systolic function and systemic blood pressure
200 regulation in aging female mice and diastolic function in aging male mice.
201
202 The cardiovascular system intricately interacts with the kidney to control blood pressure and
203 filtration, a function that is known to decline drastically with aging. HCDs have been implicated to
204 be protective of the kidney in animal models of obesity[18]. Nonetheless, N-acetylcarnosine
205 treatment did not appear to influence kidney weight (Figure 5A), histology (Figure 5B), urine
206 output (Figure 5C), creatinine clearance (Figure 5D), or glomerular filtration rates (GFR) (Figure
207 5E) in either sex (Supp. Figure 6A-G). These findings are particularly interesting given that other
208 models of HCD enrichment such as whole-body deletions of carnosinase 1 (CN1) demonstrate
209 preferential HCD enrichment in the kidney[34]. However, the GFR for both vehicle and N-
210 acetylcarnosine treated mice are similar to GFRs that of healthy young mice we reported
211 recently[35] suggesting that kidney dysfunction may not have manifested by 24 months of age.

212

213 Frailty is a hallmark of aging that very closely predicts mortality. Physical function, supported by
214 the musculoskeletal system, is known to drastically become impaired in the process of aging to
215 contribute to the decline in quality of life. Previously, we showed that N-acetylcarnosine robustly
216 attenuates muscle atrophy and weakness induced by 1-week of disuse in older mice[14]. However,
217 sarcopenia occurs gradually over a longer period, so the current study provided a perfect
218 opportunity to determine the effects of N-acetylcarnosine treatment on loss of physical function
219 with aging. N-acetylcarnosine did not appear to strongly influence muscle mass (Figure 6A) or
220 myofiber cross-sectional area in fast-twitch extensor digitorum longus (EDL) (Figure 6B&C) or
221 slow-twitch soleus muscles in either sex (Supp. Figure 7A-F). It is known that while C57Bl/6 mice
222 begin to experience atrophy at 24 months, loss of muscle mass at peaks at about 30 months of
223 age[36] so this perhaps was not too surprising. In contrast, muscle weakness precedes muscle
224 atrophy in sarcopenia[36]. Indeed, ex vivo assessment of skeletal muscle force-generating capacity
225 revealed consistent increase in both EDL and soleus muscle strength induced by N-
226 acetylcarnosine treatment in female mice (Figure 6D&E), but not in male mice (Supp. Figure
227 7G&H). A robust enrichment of N-acetylcarnosine in skeletal muscle in female mice, but not male
228 mice (Figure 1C) is consistent with these observations. Nonetheless, these improvements were
229 insufficient to be reflected in the *in vivo* assessments of physical function (Figure 6F-H, Supp.
230 Figure 7I-K). These data implicate N-acetylcarnosine as a potentially viable strategy to delay
231 features of sarcopenia in mice.

232

233 Aging also profoundly influences physical function by weakening bones, particularly in post-
234 menopausal women that experience osteoporosis. Micro-CT of femurs (Figure 7A) revealed that
235 N-acetylcarnosine treatment increased trabecular number (Figure 7B, Supp. Figure 8A) but
236 decreased trabecular spacing (Figure 7C, Supp. Figure 8B). This in parallel with unaltered
237 trabecular thickness (Figure 7D, Supp. Figure 8C) led to increased bone volume fraction (Figure

238 7E, Supp. Figure 8D) in both sexes in the distal femur. In contrast, neither tibial trabecular bone
239 nor inflammation at the knee joint were affected by N-acetylcarnosine treatment (Supp. Figure
240 8E-G). These data indicate an ability of N-acetylcarnosine to enhance bone density in the femurs
241 of aging mice.
242
243 **Discussion**
244 Aging is associated with exacerbated oxidative stress, however strategies broadly targeting
245 reactive oxidative species (ROS) have been disappointing. This may be related to the presence
246 of many primary and secondary ROS-related species and the important roles some of these
247 species play in physiological signaling and hormetic response to stress. Carbonyls may be a more
248 promising target given they are secondary ROS species, their formation is proportional to their
249 metabolite precursors which may be altered in a context-dependent manner, and they are
250 canonically not known to possess physiological signaling roles. Supplementation with HCDs such
251 as N-acetylcarnosine, carnosine, their precursor β-alanine, and synthetic analogs have
252 established efficacy for mitigating age-related pathologies such as sarcopenia[14,15], insulin
253 resistance[12,21,22], cardiovascular[33,37,38] and renal dysfunction[39] primarily in contexts outside of
254 aging purportedly via scavenging of reactive carbonyls. Ours is the first study to simultaneously
255 investigate the effects of N-acetylcarnosine on these systems during aging *per se* in a longitudinal
256 study.
257
258 Supplementation with N-acetylcarnosine improved survival of female mice by approximately 50%.
259 While the mechanism by which female mice preferentially benefited is unclear, certain tissues
260 from female N-acetylcarnosine-treated mice that displayed sex-specific effects, were more
261 enriched for N-acetylcarnosine (Figure 1C). For example, N-acetylcarnosine was only significantly
262 elevated in gWAT from female N-acetylcarnosine-treated mice (Supp. Figure 1). In parallel, we
263 observed a disparate effect of N-acetylcarnosine to promote weight retention in female mice which

264 appeared to be driven by larger gWAT (Figure 2G) without compromising metabolic function. A
265 finding in line with previous work demonstrating the ability of HCDs to protect against obesity-
266 related glucose intolerance[12,13,19]. While, the mechanism of this adipose retention is unclear, our
267 indirect calorimetry and activity data demonstrate decreased energy expenditure and activity in
268 female N-acetylcarnosine treated mice. Interestingly, recent research suggests that decreased
269 metabolic rate induced by a torpor-like state increases survivability and delays aging in mice[40].
270 Carnosine treatment has also been demonstrated to mitigate adipocyte senescence via
271 scavenging of 4-HNE in aging mice[41] which could promote retention of fat mass as we observed
272 in the N-acetylcarnosine-treated mice.
273
274 The carbonyl scavenging ability of lipid carbonyls such as 4-HNE may have also contributed to
275 vascular, muscle, and bone function as well. 4-HNE uncouples NO production in endothelial
276 cells[42] leading to impaired NO bioavailability and carnosine has been shown to facilitate NO
277 production *in vitro*[33]. While this increased NO bioavailability we observed in the N-acetylcarnosine
278 treated mice did not enhance endothelium-dependent vasodilation *ex vivo*, NO bioavailability is
279 closely associated with vascular health and appropriate blood pressure regulation which we did
280 not measure. Improved NO bioavailability may also protect old mice from additional insults (e.g.
281 ischemia reperfusion, dyslipidemia etc.) which should be tested in future experiments. It is worth
282 noting that N-acetylcarnosine drastically reduced protein carbonyl burden in the heart, even
283 though N-acetylcarnosine treated-mice did not exhibit overt improvement in heart function
284 discerned from echocardiography. However, heart functional decline likely occurs earlier than 18
285 months which may have limited the therapeutic capacity of N-acetylcarnosine in this study.
286
287 We previously found N-acetylcarnosine was effective at mitigating 4-HNE modified proteins in
288 muscle and preserved muscle force following 7-days of hindlimb unloading. Here, we demonstrate
289 that N-acetylcarnosine was effective at preserving *ex vivo* muscle force production during aging.

290 HCDs have been shown to chelate and alter the concentration of di-cations such as calcium which
291 may be an alternate mechanism to carbonyl sequestering that may have contributed to this
292 observation by altering cross bridge kinetics. This effect did not result in improved functional
293 metrics (i.e. treadmill, grip strength, rotarod) but these measurements mostly rely on submaximal
294 strength, do not necessarily reflect functional capacity relevant for trip and fall prevention
295 (important health factors for elderly individuals). Bone forming osteoblasts cells are also
296 negatively impacted by oxidative stress[43] which may have been attenuated by N-acetylcarnosine
297 treatment to increase femur trabecular bone density. Improved bone density is also translationally
298 relevant for older individuals with increased risk of bone fractures which can dramatically increase
299 morbidity and mortality especially in women. While the collection of these physiologic
300 improvements does not provide a clear explanation of why the female N-acetylcarnosine mice
301 improved survival by 50%, we speculate that the retention of adiposity may have broadly delayed
302 frailty onset which manifested with improved NO bioavailability, muscle force capacity, and bone
303 density.
304
305 In conclusion, N-acetylcarnosine treatment improves functions of multiple organ systems to
306 increase survival in female mice. As an endogenously present metabolite, N-acetylcarnosine
307 likely represents a safe, commercially scalable, and economically affordable treatment in humans.
308 The current intervention spanned 18-24 months of age, and it remains possible that N-
309 acetylcarnosine treatment has additional protective effects on age-related declines that occur
310 outside this window. Humans are known to have substantially different HCD metabolism and
311 pharmacokinetics than mice. Thus, N-acetylcarnosine is a strong candidate to be considered for
312 clinical testing to determine its efficacy in mitigating age-related health decline in humans.

313 **Methods**

314

315 **Mice**

316 All experiments were performed at the University of Utah and were approved by the Institutional
317 Animal Care and Use Committee. C57Bl/6 mice were ordered from the National Institutes on
318 Aging's aged mouse colony at 17-months of age and fed a normal chow diet, and housed with a
319 12-hour light/dark cycle in a temperature-controlled room for the duration of the study. Mice were
320 ordered in cohorts of 20 mice per months with three cohorts consisting of 10 males and 10
321 females, and five subsequent cohorts consisting of 20 female mice after observing certain trends
322 in female mice only. Upon arrival mice were weighed, counterbalanced by weight, and re-caged
323 to five mice per cage when possible and needed. Mice were monitored for the next three weeks
324 with minimum contact to allow them to acclimate to their new environment. After three weeks of
325 acclimation, baseline measures of body composition, grip strength, rotarod, and Y-Maze were
326 taken (described below).

327

328 **N-acetylcarnosine Treatment**

329 Cages of mice were randomized to receive normal drinking water (vehicle) or drinking water
330 supplemented with 80 mM N-acetylcarnosine prepared as previously described[14]. Briefly, tap
331 water was autoclaved and supplemented with N-acetylcarnosine to final concentration of 80 mM.
332 Both vehicle and N-acetylcarnosine water were titrated to a final pH of 7.5. Water was prepared
333 fresh and replaced weekly. At the time water is replaced, the mice are weighed, fresh bedding is
334 provided, and food and water consumption are measured. The intervention begins 4 weeks after
335 the mice have been acquired at 80 weeks of age and continued for 24 weeks. Over the course of
336 the intervention, mice are also monitored for general well-being and treated as needed by the
337 veterinarians. If deemed necessary by the veterinarians, mice were euthanized prior to the end
338 point. Reasons for early euthanasia included unresolving scruff wounds, anal prolapse, enlarged

339 tumors, and extreme weight loss. In addition to weekly routine monitoring, mice were assessed
340 every 8 weeks for body composition. Four weeks prior to the study endpoint, physiological
341 endpoint measures (body composition, grip strength, rotarod, treadmill test, Y-maze,
342 Comprehensive Laboratory Animal Monitoring System (CLAMS), echocardiography, 24-hour
343 urine collection, glomerular filtration rate, fear conditioning, Von Frey test, hot plate test, and
344 intraperitoneal glucose tolerance test). This timing was chosen to limit the proximity of tests to
345 one another to limit stressing the mice, and to prevent any resultant stress from confounding
346 terminal tissue collection. To limit measurement bias, the tester performing these assessments
347 was blinded and in the case of repeated measures, the same tester performed the assessment
348 at all time points.
349
350 **Body Composition**
351 Body composition was assessed at the beginning of the intervention and 8, 16, and 24 weeks of
352 treatment via Bruker Minispec NMR (Bruker, Germany).
353
354 **Grip Strength**
355 Whole body grip strength was assessed at baseline and between week 100 and 103 of the
356 intervention utilizing a grip strength meter with a mesh wire attachment (Columbus Instruments,
357 Columbus, OH, USA) with methods modified from[44]. Briefly mice were acclimated to the testing
358 room for 30 minutes. The tester then removed a mouse from the cage (blind from the group
359 allocation of that cage) and placed it onto the mesh wire attached to the dynamometer. Gripping
360 at the base of the tail, the mouse was pulled steadily, with its torso horizontal to the ground, back
361 towards the tester. This trial was repeated three times with 30 seconds between each bout and
362 the highest force being reported.
363
364 **Rotarod**

Rotarod assessment was performed at baseline and between week 100 and 103 of the intervention as previously described[44]. Briefly, mice were trained on the Rotamex-5 (Columbus Instruments, Columbus, OH) for three days prior to testing by placing mice on the apparatus at a constant speed of 4 rpm for 5 minutes, replacing them if they were to fall. On the day of testing, mice were acclimated to the testing room for 30 minutes prior to testing. After acclimating, mice were placed on the apparatus and the instrument was run at 4 rpm, accelerating 0.3 rpm/s. Mice were allowed to continue if they were able to grip the rotarod to prevent a fall. Timer continued until the mice fell to the bottom. Once the mice were assayed, the test was repeated starting with the first mouse assayed until all mice were assayed three times with the best score being reported.

Treadmill Exercise Capacity

The treadmill test was performed between week 100 and 103 of the intervention as previously described[30] prior to terminal experiments. Every day for the three days prior to the treadmill exercise test, mice were acclimated to the treadmill by placing each mouse in the treadmill for 5 minutes with the belt being stationary followed by 5 minutes with the belt running at 5 meters per minute. On the day of the test, mice were acclimated to the test room for 30 minutes. Four mice at a time were placed on the treadmill with walls separating adjacent mice. Mice began by running at 5 meters per minute at a 25% grade for 1 minute. The speed was increased by 1 meter per minute every minute until maximal exercise capacity was achieved. The mice were encouraged to run by tapping the mice with a wire cleaner brush. Maximal capacity was determined by a mouse's inability to run on the treadmill following 5 consecutive coercions with the wire brush followed by 2 attempts to place the mouse in the middle of the treadmill by hand. Maximal exercise capacity was calculated as follows:

$$Body\ Weight\ (kg) * Running\ Time\ (\text{minutes}) * \text{Final Running Speed}\ \left(\frac{\text{m}}{\text{minute}}\right) * Treadmill\ Grade\ (25\%)$$

390

391 **Y-Maze**

392 Y-Maze was performed at baseline and between week 100 and 103 of the intervention. Mice were
393 acclimated to the testing room 30 minutes prior to the assessment. The Y-maze was placed on
394 the floor in the same orientation in the same room for repeated measures. A camera was
395 suspended above the Y-maze apparatus to record the test. The mouse was then placed in the
396 center for 20 seconds of the maze with three walls blocking the path to the maze arms to acclimate
397 to the apparatus. After acclimating to the apparatus, video recording was initiated and the
398 blockades to the maze arms were removed. The branches that the mouse traveled to was
399 recorded for 15 branches unless the mouse returned to the same arm twice in a row at which
400 point the test was terminated. Spontaneous alternations were calculated by counting the number
401 of unique groupings of three arms visited across the entire test.

402

403 **CLAMS**

404 Comprehensive laboratory animal metabolic system (CLAMS, Columbus Instruments, Columbus,
405 OH) was performed between week 100 and 103 of the study to measure energy expenditure
406 (VO_2), respiratory exchange ratio (RER; VCO_2/ VO_2), food and water consumption, and physical
407 activity.

408

409 **Echocardiography**

410 Echocardiography was performed between week 100 and 103 of the study. Mice were induced
411 and maintained under light anesthesia by inhalation of isofluorane. Cardiac function was
412 measured using a VisualSonics Vevo 2100 ultrasound machine with MS400 probe. B- and M-
413 mode sequences were acquired in the parasternal long- and short-axis orientations and used to
414 assess systolic function and to quantify morphological features. Mitral inflow velocities (E and A),
415 and early diastolic mitral annulus tissue velocity (e') were measured in the apical, four-chamber

416 view using flow and tissue doppler respectively. These values were used to assess diastolic
417 function based on E/A and E/e' ratios. Echocardiographic data was analyzed using VisualSonics
418 VevoLab.
419
420 **24-Hour Urine Collection and Creatinine Clearance**
421 A 24-hour urine collection for determination of creatinine clearance was performed between week
422 100 and 103 of the study. Mice were placed in an MMC100 Metabolic Cage for 24 h at which point
423 urine and cheek blood were collected. Body weight, urine volume, food, and water intake were all
424 observed throughout the experiment. Mice were fed with a standard chow gel diet with free access
425 to water. Urine samples were centrifuged at 21,000 x g for 15 min, then aliquoted, and stored at -
426 80 C. Urine and plasma creatinine were measured using QuantiChrom Creatinine Assay Kit,
427 BioAssay Systems, Hayward, CA (Cat. No. DIUR-500) according to the manufacturer's
428 instructions. Creatinine clearance was calculated as follows:

429 $$\frac{Urine\ Creatinine\ Concentration\ \left(\frac{mg}{dL}\right) * Urine\ Volume\ (mL)}{Plasma\ Creatinine\ Concentration\ (\frac{mg}{dL})}$$

430
431 **Glomerular Filtration Rate**
432 Glomerular filtration rate (GFR) was measured between week 100 and 103 of the study as
433 previously described[45]. Mice were injected with fluorescein isothiocyanate-senestrin
434 (Medibeacon, Mannheim, Germany) retro-orbitally (7.5 mg/100 g body weight). The NIC-Kidney
435 (Medibeacon) was used to detect fluorescence in the skin on the shaved back over 1 h. GFR was
436 calculated based on the kinetics of fluorescence decay as previously reported[46].
437
438 **Fear Conditioning**

Fear conditioning was conducted between week 100 and 103 of the study using a med-associates sound-attenuated chamber (29x25x26 cm) with no scent, plexiglass roof and front door, aluminum side walls, a plastic black wall and fitted with a top-down camera (*Context A)* (Med Associates; St. Albans, Vermont). Conditional and contextual memory were assessed on two subsequent days. On day 1 mice were acclimated to the test room for at least 1 hour. After shock calibration, an individual mouse was placed in the chamber for 3 minutes. At 120 seconds, a tone was delivered for 20 seconds. Two seconds prior to termination of the tone, a 0.3 mA foot shock was delivered lasting 2 seconds. The mouse remains in the chamber until the end of the 3 minutes. The mouse is then returned to its cage, and the chamber is cleaned with 70% ethanol before testing the next mouse. On day 2, contextual fear conditioning is tested by introducing mice to *Context A* for 3 minutes without tone or shock. The percent time freezing on day 1 and day 2 are reported as metrics of contextual memory. One hour later, mice are tested for conditional memory by being introduced to a new context which differs from *Context A* by placing curved plastic board inside the chamber, a plastic board underneath the grid floor, and the chamber is scented with vanilla extract (*Context B)*. Mice are allowed to explore for 3 minutes without foot shocks but with the same tone as on the first day occurring during the last minute. The percent change (%Δ) of time freezing before and after the tone on day 1 compared to day 2 is reported as the metric for conditional memory.

Von Frey Test

The Von Frey test was performed between 100 and 103 weeks of the study. Mice were acclimated to the procedure room for 30 minutes prior to testing. Mice were placed in a small chamber with grid wire flooring. The Von Frey apparatus was fitted with three filaments of different tensions. These filaments were applied to the plantar region of the mouse's foot and the force needed to elicit withdraw of the foot is recorded. Each test was repeated three times with 15 minutes between each test.

465

466 **Hot Plate Test**

467 The hot plate test was performed between 100 and 103 weeks of the study. Mice were acclimated
468 to the procedure room for 30 minutes prior to testing. A glass enclosure was warmed to 50 degrees
469 Celsius and a camera was affixed to record the animal's behavior in response to being placed in
470 the enclosure. Change in behavior indicating pain (e.g. picking up paws, rearing etc.) was scored
471 and timed by 3 independent and blinded individuals.

472

473 **Terminal Biological Sample Collection**

474 On week 104, 4-hour fasted mice were anesthetized via intraperitoneal injection of 80 mg/kg
475 ketamine and 10 mg/kg xylazine. Hindlimb muscles (Tibialis anterior [TA], Extensor digitorus
476 longus [EDL], soleus, plantaris, and gastrocnemius) were quickly collected from live mice,
477 weighed, and either tied with sutures on distal and proximal tendons for *ex vivo force* (EDL and
478 soleus; described below), flash frozen in liquid nitrogen, or embedded in OCT and frozen in liquid
479 nitrogen-cooled isopentane for histological assessment (described below). After collecting
480 muscles, blood was collected via cardiac puncture followed by collecting, weighing, preservation
481 of the remainder of the tissues (heart, liver, kidney, inguinal white adipose tissue [iWAT], gonadal
482 [gWAT], brain, sperm, and bones).

483

484 **Targeted Metabolomics**

485 Plasma, urine, muscle (TA), whole brain, heart, iWAT, gWAT, kidney, and liver were processed
486 from frozen and assessed for N-acetylcarnosine, carnosine, histidine, anserine, and
487 homocarnosine concentrations. Sample preparation and metabolomics methods were based on
488 recently published protocols[4].

489

490 Frozen tissues were quickly weighed and immediately placed in HPLC-grade water with 10 mM
491 HCl (12 µL extraction solution per mg tissue) followed by homogenization in a bead mill
492 homogenizer at 4°C. Homogenates were centrifuged (20 min, 3000 × g, 4°C) and the resulting
493 supernatants were immediately diluted in a 3:1 ratio with ice-cold acetonitrile. The mixture was
494 vortexed for 15 s and kept on ice for 15 min. After a second centrifugation step (12 min, 20,000 ×
495 g, 4°C), samples were stored at −80°C until the day of analysis. Plasma and urine samples (37.5%
496 of total mixture) were combined with acetonitrile containing 1% formic acid (54%) and HPLC-
497 grade water (8.5%). Samples were vortexed for 15 s and centrifuged (15 min, 15,000 × g, 4°C),
498 after which supernatant was collected and stored at −80°C until the day of analysis.
499
500 Targeted metabolite measurements were performed on a triple quadrupole LC-MS instrument
501 (Agilent 6470). Normal phase chromatography was used to separate polar metabolites using a
502 Luna 5µm NH_2 100 Å LC column (Phenomenex 00G-4378-E0) equipped with a SecurityGuard
503 cartridge (KJ0-4282, Phenomenex). Injection volume was 7 µL, except for urine (4 µL). Mobile
504 phases consisted of Buffer A (water with 10 mM ammonium formate) and Buffer B (95:5
505 acetonitrile:water with 10 mM ammonium formate). Each run started 100% B for 2 minutes,
506 followed by a gradient starting at 100% B changing linearly to 50% A and 50% B over the course
507 of 10 minutes, followed by 50% A and 50% B for 3 minutes, and re-equilibration at 100% B for 2
508 min (flow rate 0.7 mL/miN). MS analysis was performed using AJS in positive mode with the
509 following parameters: dry gas temperature 250 °C, gas flow 12 L/min, nebulizer pressure 25 psi,
510 sheath gas temperature 300 °C, the sheath gas flow 12 L/min, capillary voltage 3,500 V. Multiple
511 reaction monitoring was performed to detect N-acetylcarnosine (269.1 → 110.1 *m/z*), carnosine
512 (227.1 → 110.1 *m/z*), anserine (241.1 → 109.1 *m/z*), homocarnosine (241.1 → 110.1 *m/z)*,
513 histidine (156.1 → 110.1 *m/z*). Secondary transitions[4] were used as confirmation of the peak
514 identity. Fragmentor voltage for the various metabolites was 80-100, collision energy 10-24 V.
515 Endogenous metabolite concentrations were quantified using an external standard curve with

516 known concentrations analyzed alongside the biological samples in the same run, except for
517 homocarnosine. Total peak areas were used to calculate metabolite concentrations within each
518 sample.
519
520 **Protein Carbonyl Assay**
521 Protein carbonyls were measured via DNPH derivatization of proteins from tissues lysed in 50
522 mM MES buffer pH 7.4, 50 mM EDTA via protein carbonyl colorimetric assay kit (10005020,
523 Caymen Chemical, Ann Arbor, MI).
524
525 ***Ex Vivo* Muscle Force**
526 Force generating capacity of both the soleus and EDL were measured as previously
527 described[14,47-49]. Briefly, soleus and EDL were tied with suture at proximal and distal tendons then
528 attached to an anchor and force transducer in a tissue bath (Aurora Scientific, Model 801C) while
529 being submerged in oxygenated Krebs-Henseleit Buffer solution at 37° C. The optimal length of
530 the muscle was determined via maximum twitch force production. The buffer was then replaced
531 with a fresh buffer solution and equilibrated for 5 minutes. After equilibration, a force-frequency
532 sequence stimulated the muscle at increasing frequencies (10, 20, 30, 40, 60, 80, 100, 125, 150,
533 and 200 Hz) with a 2-minute rest interval between each frequency. The rates of contraction and
534 relaxation were quantified as previously described[14,47,48]. The Aurora Scientific DMAv5.321
535 software was utilized for analysis of force production data.
536
537 **Muscle Histology and CSA**
538 OCT embedded soleus and EDL samples were mounted on a precooled platform and sectioned
539 at 10 μm thickness with a cryostat (Microtome Plus). 6-8 serial sections from each sample were
540 transferred onto the same slide. Sections then underwent blocking for 1 hour at room temperature
541 with M.O.M. mouse IgG blocking reagent (Vector Laboratories, MKB-2213), after which they were

542 incubated overnight at 4° C with a concentrated primary antibody targeting laminin (1:200, Sigma,
543 L9393) in 2.5% horse serum in PBS. The next day, sections were incubated for 1 hour at room
544 temperature with anti-rabbit IgG conjugated to Alexa Fluor 647 (1:250, Invitrogen, A21245).
545 Sections were then washed three times in PBS, fixed with methanol for 5 minutes at room
546 temperature and then washed 2 more times in PBS. Finally, slides were mounted with mounting
547 medium (Vector 136 Laboratories, H-1000). Slides were imaged on a Zeiss Axioscan.Z1 at 20X
548 magnification. Masks for fibers were generated via Cellpose (V3.0)[50] and then imported into
549 ImageJ software where CSA was quantified.
550
551 **Tissue H&E and Trichrome Staining**
552 Portions of tissues (e.g. liver, heart) or antiliteral tissues (e.g. kidney) that were not flash frozen in
553 liquid nitrogen, were taken from each mouse and immediately submerged in 4%
554 paraformaldehyde for 12 hours and then 70% ethanol for 48 hours. Tissues were sectioned were
555 then embedded in paraffin, sectioned at 10-µm thickness, stained for Masson's Trichrome to
556 assess fibrosis or hematoxylin and eosin (H&E) to determine fat droplet accumulation and general
557 morphological features. Samples were imaged on Axio Scan Z.1 (Zeiss).
558
559 ***Ex Vivo* Vascular Function**
560 Vasocontractile responses to potassium chloride (KCl, 20–100 mM) and phenylephrine (PE, 10^{-8}-
561 10^{-5} M; not shown), and vasorelaxation responses to acetylcholine (10^{-8}-10^{-5} M] and sodium
562 nitroprusside (10^{-9}-10^{-4} M; not shown), were completed using isometric myography as we have
563 described[51]. To determine the contribution to vasorelaxation from endothelial nitric oxide synthase
564 (eNOS), a second Ach dose-response curve was completed (30-min later) in the presence of the
565 eNOS inhibitor NG methyl L arginine acetate salt (L-NMMA; 1mM]. To calculate NO bioavailability
566 for each group, maximal vasorelaxation to Ach in the presence of L-NMMA was subtracted from
567 maximal vasorelaxation to Ach in the absence of L-NMMA, and all values were averaged, and

568 compared between groups. For all responses, values from two femoral artery segments per
569 mouse were averaged.
570
571 **Knee Joint Histology and Scoring**
572 To evaluate the effects of N-acetylcarnosine on OA development in aged mice right hind limbs
573 were collected and fixed in 10% formalin. Bone microstructure analysis was performed as stated
574 below. Following bone microarchitecture analysis by micro-CT joints were decalcified,
575 dehydrated, and embedded in paraffin. The joint was sectioned at a thickness of 8 μm. To
576 determine OA severity, joint sections were stained with hematoxylin, fast green, and Safranin-O.
577 Three independent, blind graders scored joint sections for OA using a modified Mankin scoring
578 system (Glasson, 2007). Scores were averaged among graders for the whole joint.
579
580 **Distal Femur Micro-Computed Tomography**
581 Femur bone structure and morphological changes were measured using a Siemens Inveon®
582 Multi-Modality microPET/SPECT/CT machine using the following imaging parameters: an X-ray
583 tube potential of 80 kVp, an X-ray tube current of 100 μA, an integration time of 2600 ms, and an
584 isotropic voxel size of 10 μm. Image analysis was performed using Inveon® Research Workplace
585 (IRW) 4.0. A 100-slice volume of interest (VOI) was selected for the cortical bone, centered about
586 the mid-diaphysis. Cortical bone was delineated from the medullary cavity using a fixed threshold
587 that remained constant across specimens. A second 100-slice VOI was selected for the trabecular
588 bone, beginning just proximal to the distal epiphyseal plate and extending into the metaphysis.
589 Irregular anatomical contours were drawn slice-by-slice throughout this VOI just within the
590 endocortical boundary as described by Bouxsein and colleagues[52]. Trabecular bone was
591 delineated from the medullary cavity using a fixed threshold that remained constant across
592 specimens. IRW's *Bone Morphometry* tool was used to compute bone volume fraction, trabecular
593 spacing, trabecular thickness, and trabecular number. The *Annotation and Measurement* tool was

594 used to estimate the cortical thickness from four measurements at the mid-diaphysis
595 (corresponding to the major and minor axes of an ellipse approximating the cross-section of the
596 femur).
597
598 **Proximal Tibia Micro Computed Tomography**
599 Tibial bone structure and morphological changes were measured in the intact hind limbs of mice
600 by micro-CT (PerkinElmer Quantum GX2 microCT) with a 5.5-μm isotropic voxel resolution.
601 Subchondral/trabecular regions were segmented using CTAn automatic thresholding software.
602 The tibial and femoral epiphyses were selected using the subchondral plate and growth plate as
603 references. The tibial metaphysis was defined as the 300 μm region directly below the growth
604 plate. Micro-CT limb images were analyzed for bone volume/total volume (BV/TV), trabecular
605 bone number (Tb.N), trabecular bone thickness (Tb.TH), trabecular bone separation (Tb.SP)[53].
606
607 **Statistics**
608 Significance for all statistical comparisons was set at $p<0.05$. Data were tested for normal
609 distribution via visual inspection of QQ plots for linearity. Student's T test or Wilcoxon Signed Rank
610 test were used for comparison of two groups depending on normality of data. Repeated
611 measurements, two-way ANOVAs or if some repeated measures were missing, mixed effects two-
612 way ANOVAs were utilized to test group by time interactions with Bonferroni Post Hoc analyses
613 applied where appropriate. Individual sample values as well as estimates of central tendency
614 (mean or media where indicated) are presented in all bar graphs. Standard error of the mean is
615 reported as the variance metric. Z-scores for radar plots in Figure 1 were calculated by
616 considering the distribution of all samples regardless of sex or group. Statistical analyses
617 including two-way ANOVA, mean, and SEM for these data are presented in Supp. Figure 1.
618

619 **Data Availability**

620 Raw data will be available with reasonable request to the corresponding author.

621

622 **Ethics Declaration**

623 The authors declare no competing interests.

624

625 **Author Contributions**

626 ERM conceived of and designed the study, conducted experiments, performed data analysis, and
627 wrote and edited the manuscript. KF conceived of and designed the study, analyzed data, and
628 wrote and edited the manuscript. MJD and AC conceived of and designed the study, analyzed
629 data, and edited the manuscript. JLS, SW, JS, SM, IYG, TS, MRG, SB, NSH, JDS, and JZL
630 conducted experiments, analyzed data, and edited the manuscript. NYM, GN, BW, DS, JW, MJ,
631 GH, TK, JKL, BR, KTO, NJB, HL, LSN, YL, CFD, JEC, CMK, NR conducted experiments and
632 analyzed data.

633

634 **Acknowledgements**

635 This work was supported by NIH grants DK110858 (JEC); HL167866, DK128819 (SB);
636 AR083904, AR071967 (CMK); DK133271 (NR); NS137105 (JDS); AG065993, CA272529,
637 CA286584 (AC); DK130641, MH133313, DK136526, OD034455, DK124265 (JZL); AG074535,
638 AG076075 (MJD); AG074535, DK127979, DK107397, GM144613 (KF); HL007576 (ERM);
639 DK137475 (MRG); AHA predoctoral grant AHA1025910, University of Utah Graduate Research
640 Fellowship (SM); and the grant-in-aid for Japan Society for Promotion of Science (JSPS) Fellows
641 24KJ2039 (TK). Figures were edited by Nikita Abraham. This work was also supported by the
642 following University of Utah Core Facilities: Cell Imaging Core, Preclinical Imaging Core, and
643 Metabolic Phenotyping Core.

644

Figure Legends

Figure 1 – N-acetylcarnosine supplementation preferentially improves female mouse survival.

A) Schematic of the preclinical trial design. C57Bl/6 mice from the NIA aging colony were acquired at 17 months of age. After acclimation, mice underwent baseline testing before being randomized to receive either vehicle or N-acetylcarnosine-supplemented water for 6 months. Mice were weekly monitored for body weight and food and water consumption. Various physiologic tests were conducted during the 5th month of the intervention. Mice were euthanized and tissues were harvested after 6 months of intervention period. **B)** Schematic representation of HCD metabolism. Radar plots of **C)** N-acetylcarnosine, **D)** protein carbonyls, **E)** Carnosine, **F)** Histidine, **G)** Anserine, and **H)** Homocarnosine demonstrate enrichment of N-acetylcarnosine. Values in radar plots are Z-scores. Corresponding concentrations and statistical analyses are in **Supplemental Figure 1**. Vehicle treated female **(I)** and male **(J)** mice experienced typical survival rates for this strain and colony (approximately 50% and 75% respectively) at 24 months. Female mice (starting n=45 vehicle, n=46 N-acetylcarnosine) treated with N-acetylcarnosine improved their survival probability by ~50%. Statistical testing for HCD enrichment was performed via two-way repeated measures ANOVA with Bonferroni post-hoc test where appropriate. Survival was assessed via generating Kaplan-Meier survival curves and testing the disparity of the curves via Mantel-Cox test. Comparisons were considered statistically significant if $p<0.05$. HCD; Histidine Containing Dipeptide, GABA; gamma-aminobutyric acid, CN1; carnosinase 1, CARNS; carnosine synthase. Schematic images were generated via BioRender.

Figure 2 – N-acetylcarnosine supplementation preserves body mass in female mice.

Body weights in the female (starting n=39 vehicle, n=40 N-acetylcarnosine) **(A)** and male (starting n=20 per group) **(B)** mice fell precipitously over the course of the trial regardless of treatment. Female mice treated with N-acetylcarnosine were able to delay the decrease in bodyweight. Bodyweights are reported as one-month averages and are presented as Mean ± SEM. N-acetylcarnosine did not affect lean mass in female **(C)** or male **(D)** mice. N-acetylcarnosine preserved fat mass in female mice **(E)** (n=57 per group) but not male **(F)** (n=20 per group) mice. **G)** Preservation of fat mass in female mice was attributed to larger gWAT not iWAT or BAT fat pad (n=16 vehicle, n=20 N-acetylcarnosine). **H)** H&E stain of gWAT tissues did not reveal differences in adipocyte size between groups. Despite increased adiposity, liver weight **(I)** was not altered by N-acetylcarnosine (n=15 vehicle, n=20 N-acetylcarnosine. **J)** H&E and trichrome stains did not indicate altered steatosis or fibrosis in livers. Statistical testing for bodyweight and body composition comparisons was performed via one-way repeated measures ANOVA with Bonferroni post-hoc test where appropriate. Statistical testing for comparison of tissue weights was performed via unpaired student t-test. Comparisons were considered statistically significant if $p<0.05$. gonadal white adipose tissue; gWAT, inguinal white adipose tissue; iWAT, Brown Adipose Tissue; BAT.

Figure 3 – N-acetylcarnosine supplementation does not alter metabolic or neuroendocrine system in female mice.

A) Glucose tolerance via intraperitoneal glucose tolerance test (IPGTT) was not different between treatment and vehicle mice (n=6 vehicle, n=9 N-acetylcarnosine). 72-hour indirect calorimetry revealed suppressed energy expenditure (VO_2) **(B)** and respiratory exchange ratio (RER) **(C)**

688 during both light and dark phases (n=5 vehicle, n=8 N-acetylcarnosine). Respiratory exchange
689 ratio is the volume of CO_2 consumed (VCO_2) proportional to the O_2 consumed (VO_2) and indicates
690 substrate utilization whereby a value closer to 0.75 indicates complete reliance on fat oxidation
691 and a value closer to 1 indicates complete reliance on glucose oxidation. Ambulatory frequency
692 was also suppressed in N-acetylcarnosine mice **(D)** (n=5 vehicle, n=8 N-acetylcarnosine). **E)**
693 Brain weights were not different between treatment groups (n=14 vehicle, n=19 N-
694 acetylcarnosine). **F)** Change in time spent freezing before and after an audible tone that
695 proceeded with a shock on the first (condition day) but not the second (follow up) day was not
696 different between groups indicating no effect of N-acetylcarnosine on conditional memory
697 formation (n=5 vehicle, n=9 N-acetylcarnosine). **G)** Frequency of novel, non-consecutive
698 exploration (alterations) between arms in the Y-maze was not different between groups indicating
699 no effect of N-acetylcarnosine on short-term memory (n=20/14 pre/post vehicle, n=20/16 pre/post
700 N-acetylcarnosine). **H)** Peripheral pain tolerance assessed via Von Frey hair filaments were not
701 different between groups (n=5 vehicle, n=9 N-acetylcarnosine). Data are represented as Mean ±
702 SEM. Statistical significance was assessed via two-way repeated measures ANOVA with
703 Bonferroni correction, or unpaired t-test where appropriate. Comparisons were considered
704 statistically significant if $p<0.05$. RER; respiratory exchange ratio, CLAMS; comprehensive lab
705 animal monitoring system.

706 **Figure 4 – N-acetylcarnosine supplementation improves cardiovascular function in female**
707 **mice.**

708 **A)** Heart weight normalized to tibial length was not different between groups of female mice. **B)**
709 H&E staining of heart tissues was also indiscernible between groups. **C)** Heart rate measured via
710 electrocardiogram was performed on anesthetized mice during echocardiography and was not
711 different between groups. Metrics of systolic function including cardiac output **(D)** and ejection
712 fraction **(E)** were not different between groups whereas fractional shortening was reduced by N-
713 acetylcarnosine treatment **(F)**. Measures of diastolic function including E/A (ventricular filling) **(G)**
714 and E/e' (marker of left ventricular filling pressures) **(H)** were not different between groups.
715 Isolated femoral arteries (n=8 vehicle, n=15 N-acetylcarnosine, 2 segments per mouse) were pre-
716 contracted to 65% of maximal developed tension, and vasorelaxation to cumulative doses of Ach
717 was recorded as percent (%) vasorelaxation. No differences were observed between groups. A
718 second Ach dose-response curve was completed (30-min later) in arteries from both groups that
719 incubated with LNMMA for 30-min. While L-NMMA attenuated vasorelaxation in arteries from
720 vehicle and N-acetylcarnosine-treated mice, the contribution from NO to vasorelaxation was
721 greater in the latter group **(I)**, an observation that was substantiated by calculating NO
722 bioavailability **(J)**. Data are represented as Mean ± SEM. Statistical significance was assessed
723 via two-way repeated measures ANOVA with Bonferroni correction, or unpaired t-test where
724 appropriate. Comparisons were considered statistically significant if $p<0.05$. Heart Rate; HR.

725 **Figure 5 – N-acetylcarnosine supplementation does not alter renal function in female mice.**

726 Kidney weight was not different between groups **(A)**. H&E and Trichrome stains of kidney sections
727 were unremarkable and indistinguishable between groups **(B)**. Mice were placed in single housed,
728 urine collection chambers for 24 hours to collect 24-hour urine volume which was not different
729 between groups **(C)**. 24-hour urine and plasma and urine creatinine concentration were used to
730 determine creatinine clearance **(D)** which also was not affected by N-acetylcarnosine. Glomerular
731 filtration determined by monitoring the filtration of a FIT-c labeled senestrin under anesthesia was
732 also not different between groups in female mice (n=5 vehicle, n=7 N-acetyl carnosine) **(E)**. Data

are represented as Mean ± SEM. Statistical significance was assessed via two-way repeated measures ANOVA with Bonferroni correction, or unpaired t-test where appropriate. Comparisons were considered statistically significant if $p<0.05$.

Figure 6 – N-acetylcarnosine supplementation improves muscle function in female mice.

A) Lower hind limb weights were not different between groups (n=23-24 vehicle, n=35-37 N-acetylcarnosine) with the exception of gastrocnemius (Gast). **C)** Histogram of the frequency of fibers sizes was not different between groups in EDL (n=6 vehicle, n=8 N-acetylcarnosine). **D)** Representative image of immunofluorescent stain for laminin used to determine muscle cross sectional area in the EDL. E*x vivo specific* force measured in EDL **(E)** (n=8 vehicle, n=8 N-acetylcarnosine) and SOL **(F)** (n=8 vehicle, n=9 N-acetylcarnosine) were elevated in N-acetylcarnosine-treated mice across stimulation frequencies ranging from 10-200 Hz. *In vivo* functional data as quantified by rotarod **(G),** grip strength **(H)**, and treadmill work capacity **(I)** were unaffected by N-acetylcarnosine treatment. Data are represented as Mean ± SEM. Statistical significance was assessed via two-way repeated measures ANOVA or two-way ANOVA with Bonferroni correction, or unpaired t-test where appropriate. Comparisons were considered statistically significant if $p<0.05$. Tibialis anterior; TA, plantaris; Plant, gastrocnemius; Gast, extensor digitorum longus; EDL, soleus; SOL.

Figure 7 – N-acetylcarnosine supplementation improves bone density in female mice.

A) Representative µCT image of femur analyzed for bone density in the distal femur. µCT of femurs revealed increased trabecular number **(B)** and decreased trabecular spacing **(C)** without a change in trabecular thickness **(D)** which contributed to a near-significant increase in the proportion of bone volume **(E)** in the ROI. Data are represented as Mean ± SEM. Statistical significance was assessed via unpaired t-test where appropriate. Comparisons were considered statistically significant if $p<0.05$. Cross sectional area; CSA, micro computed tomography; µCT.

Supplemental Figure 1 – Histidine-containing dipeptides and protein carbonyl concentrations across tissues.

Targeted metabolomics via LC-MS was utilized to quantify N-acetylcarnosine, carnosine, anserine, histidine, and homocarnosine in plasma, urine, muscle (TA – HCDs, Gastroc. – carbonyls), brain (cortex), heart (ventricle), kidney, liver, iWAT, and gWAT. Data are presented as Mean ± SEM. Two-way ANOVA was used to test statistical significance. The p-values for the main effects of N-acetylcarnosine treatment (Treatment), sex, and the interaction of these variables (sex x treatment) are reported in the last three columns respectively. Significance was set a $p<0.05$. Bolded *p*-values indicate a significant main effect.

Supplemental Figure 2 – N-acetylcarnosine supplementation does not alter food or water intake.

Free-living female food **(A)** and water **(B)** and male food **(C)** and water **(D)** were not different on a per cage basis. Data are represented as mean ± SEM of the grams of consumption per mouse per day. Food **(E)** and water **(F)** consumption was also determined during the CLAMS (n=8 vehicle, n=8 N-acetylcarnosine) assessment of single-housed mice. Food consumption was only significantly increased in male mice during the dark phase. Data are presented as Mean ± SEM. Statistical significance was assessed by two-way repeated measures ANOVA with Bonferroni post-hoc where appropriate. Significance was set to $p < 0.05$).

Supplemental Figure 3 – N-acetylcarnosine supplementation does not glucose tolerance and attenuates energy expenditure.

A) Male iWAT, gWAT, and liver weights were not different between groups. **B)** H&E and Trichrome stains of liver sections in male mice were not remarkably different between groups demonstrating limited lipid infiltration and fibrosis in both groups. **C)** 2-hour IPGTT revealed no differences in plasma glucose in male mice at any time point or as represented as area under the curve (AUC) **(D)**. **E)** CLAMS revealed a trend for lower hourly energy expenditure (relative VO_2), and a significantly lower energy expenditure AUC in the N-acetylcarnosine treated male mice in the light and dark time points **(F)**. **G)** Hourly ambulation (3h averages) and RER **(H)** in male mice was not different between groups during CLAMS. Ambulation AUC was significantly higher in the male, N-acetylcarnosine treated mice **(I)** in light and dark time points. **J)** Motion in the Z-direction was not affected by N-acetylcarnosine in the male mice. **K)** Female glucose AUC during 2-hour IPGTT was not different between groups. **L)** Female energy expenditure (relative VO_2) AUC was lower in N-acetylcarnosine treated mice. **M)** Total ambulation was lower in light and dark time points in female N-acetylcarnosine treated mice. **N)** Z-motion frequency was not different between female vehicle and N-acetylcarnosine-treated mice. Data are presented as Mean ± SEM. Two-way RMANOVA or T-tests were used for statistical comparison with Bonferroni post-hoc test where appropriate. Comparisons were considered statistically significant if $p<0.05$.

Supplemental Figure 4 – N-acetylcarnosine supplementation does not improve male reproductive health or male and female neurophysiology.

Sperm collected from the epididymis of male mice were collected and a sperm count was performed at the time of euthanasia. **A)** N-acetylcarnosine did not affect total, dead, or alive sperm counts. **B)** Brain weights, and cognition as assessed by contextual and conditional fear conditioning **(C and D)** were not affected by N-acetylcarnosine in male mice. **E)** Peripheral pain perception as assess by Von Frey assessment were not affected by N-acetylcarnosine treatment

in male mice. Like male mice, contextual fear conditioning **(F)** was not affected by N-acetylcarnosine. **G)** Hot plate assay like Von Frey indicated no effect of N-acetylcarnosine in peripheral nociception in female mice. Data are presented as mean ± SEM and assessed by ttest or 2-way RMANOVA with Bonferroni correction applied for post hoc testing where appropriate. Comparisons were considered statistically significant if $p<0.05$.

Supplemental Figure 5 – N-acetylcarnosine supplementation improves diastolic function in male mice.

A) Heart weight relative to tibia length was not different between groups in male mice. Echocardiographic assessment (n=12 vehicle, n=13 N-acetylcarnosine) of mouse systolic function **(B-E)** was also not affected by N-acetylcarnosine in male mice. Early stage **(F)** left ventricular filling was also not different but late diastolic filling **(G)** was greater in N-acetylcarnosine-treated male mice indicating some mild improvements in diastolic function in male mice. **H)** Heart histology as assessed by H&E staining was morphologically similar between groups. Data are presented as mean ± SEM and assessed by unpaired t-test whereby comparisons were considered statistically significant if $p<0.05$.

Supplemental Figure 6 – N-acetylcarnosine supplementation does not affect renal function in male mice.

A) Kidney weight relative to body mass was not different in male mice. 24-hour urine collection was conducted in a modified single mouse cage. **B)** Urine volume trended higher but was not significant in N-acetylcarnosine-treated male mice whereas plasma creatinine concentrations **(C)** trended lower and creatinine clearance **(D)** was equivocal between groups in male mice. **E)** GFR was determined in a subset of male mice (n=6 vehicle, n=6 N-acetylcarnosine) by measuring the excretion of FIT-c labeled senestrin into the urine and was not different between groups. Kidney H&E **(F)** and trichrome **(G)** did not reveal obvious differences in kidney morphology or fibrosis between groups. Data are presented as mean ± SEM and assessed by unpaired t-test whereby comparisons were considered statistically significant if $p<0.05$.

Supplemental Figure 7 – N-Acetylcarnosine supplementation does not dramatically alter muscle function in male mice.

A) CSA frequency and **(B)** representative image of soleus cross section from female mice demonstrate the frequency of soleus muscle fibers trended smaller in N-acetylcarnosine treated female mice (n=7 vehicle, n=6 N-acetylcarnosine). **C)** Hindlimb muscle weights are not affected by N-acetylcarnosine in male mice. **D)** Representative image of soleus and EDL muscles cryosectioned and stained for laminin for determination of muscle fiber cross sectional area (CSA). **E)** Frequency of larger fibers is increased in EDL muscles from N-acetylcarnosine treated male mice whereas no such effect was found in soleus **(F)**. *Ex vivo* specific force assessed in EDL **(G)** and soleus **(H)** muscles were also not different between groups in male mice. Despite greater CSA in EDL, rotarod **(I)**, grip strength of all four limbs **(J)**, and treadmill work capacity **(K)** were not affected by N-acetylcarnosine treatment. Data are presented as mean ± SEM and assessed by t-test or two-way repeated-measures ANOVA with Bonferroni correction applied for post hoc testing where appropriate. Comparisons were considered statistically significant if $p<0.05$.

Supplemental Figure 8 – N-acetylcarnosine supplementation improves bone density in femurs from male mice but does not affect knee joint inflammation or tibia bone density.

Micro-CT (μCT) analysis of femur bones demonstrated increased trabecular number **(A)**, decreased trabecular spacing **(B)**, no change in trabecular thickness **(C)**, and increased bone volume fraction **(D)** collectively indicating greater bone density in male N-acetylcarnosine treated mice. **E)** Representative images of safranin-O-stained knee joints subjected to Mankin scoring (n=10 vehicle, n=17 N-acetylcarnosine, not significant, data not shown). Representative μCT images of the whole knee joint **(F)** and the tibial epiphysis **(G)**. Trabecular number, spacing, thickness**,** and bone volume were not different between groups by μCT. Data are presented as mean ± SEM and assessed by t-test or two-way repeated-measures ANOVA with Bonferroni correction applied for post hoc testing where appropriate. Comparisons were considered statistically significant if $p<0.05$.

References

1 Mattison, J. A. *et al.* Caloric restriction improves health and survival of rhesus monkeys. *Nat Commun* **8**, 14063, doi:10.1038/ncomms14063 (2017).

2 Colman, R. J. *et al.* Caloric restriction delays disease onset and mortality in rhesus monkeys. *Science* **325**, 201-204, doi:10.1126/science.1173635 (2009).

3 Ruegsegger, G. N. & Booth, F. W. Health Benefits of Exercise. *Cold Spring Harb Perspect Med* **8**, doi:10.1101/cshperspect.a029694 (2018).

4 Van der Stede, T. *et al.* Extensive profiling of histidine-containing dipeptides reveals species- and tissue-specific distribution and metabolism in mice, rats, and humans. *Acta Physiol (Oxf)* **239**, e14020, doi:10.1111/apha.14020 (2023).

5 Saunders, B. *et al.* beta-alanine supplementation to improve exercise capacity and performance: a systematic review and meta-analysis. *Br J Sports Med* **51**, 658-669, doi:10.1136/bjsports-2016-096396 (2017).

6 Kameda, M., Teruya, T., Yanagida, M. & Kondoh, H. Frailty markers comprise blood metabolites involved in antioxidation, cognition, and mobility. *Proc Natl Acad Sci U S A* **117**, 9483-9489, doi:10.1073/pnas.1920795117 (2020).

7 Aldini, G., Carini, M., Beretta, G., Bradamante, S. & Facino, R. M. Carnosine is a quencher of 4-hydroxy-nonenal: through what mechanism of reaction? *Biochemical and Biophysical Research Communications* **298**, 699-706, doi:10.1016/S0006-291X(02)02545-7 (2002).

8 Czyzowska, A. *et al.* Elevated phospholipid hydroperoxide glutathione peroxidase (GPX4) expression modulates oxylipin formation and inhibits age-related skeletal muscle atrophy and weakness. *Redox Biol* **64**, 102761, doi:10.1016/j.redox.2023.102761 (2023).

9 Fritz, K. S. *et al.* 4-Hydroxynonenal Inhibits SIRT3 via Thiol-Specific Modification. *Chem Res Toxicol* **24**, 651-662, doi:10.1021/tx100355a (2011).

10 Coliva, G., Duarte, S., Perez-Sala, D. & Fedorova, M. Impact of inhibition of the autophagy-lysosomal pathway on biomolecules carbonylation and proteome regulation in rat cardiac cells. *Redox Biol* **23**, 101123, doi:10.1016/j.redox.2019.101123 (2019).

11 Wang, Q. *et al.* The impact of carnosine on biological ageing - A geroscience approach. *Maturitas* **189**, 108091, doi:10.1016/j.maturitas.2024.108091 (2024).

12 Anderson, E. J. *et al.* A carnosine analog mitigates metabolic disorders of obesity by reducing carbonyl stress. *J Clin Invest* **128**, 5280-5293, doi:10.1172/JCI94307 (2018).

13 de Courten, B. *et al.* Effects of carnosine supplementation on glucose metabolism: Pilot clinical trial. *Obesity (Silver Spring)* **24**, 1027-1034, doi:10.1002/oby.21434 (2016).

14 Eshima, H. *et al.* Lipid hydroperoxides promote sarcopenia through carbonyl stress. *eLife* **12**, e85289, doi:10.7554/eLife.85289 (2023).

15 del Favero, S. *et al.* Beta-alanine (Carnosyn™) supplementation in elderly subjects (60-80 years): effects on muscle carnosine content and physical capacity. *Amino Acids*, 49-56, doi:10.1007/s00726-011-1190-x (2012).

16 Baba, S. P. *et al.* Evaluation of supplementary carnosine accumulation and distribution: an initial analysis of participants in the Nucleophilic Defense Against PM Toxicity (NEAt) clinical trial. *Amino Acids* **56**, 55, doi:10.1007/s00726-024-03414-5 (2024).

17 Turturro, A. *et al.* Growth curves and survival characteristics of the animals used in the Biomarkers of Aging Program. *J Gerontol A Biol Sci Med Sci* **54**, B492-501, doi:10.1093/gerona/54.11.b492 (1999).

18 Aldini, G. *et al.* The carbonyl scavenger carnosine ameliorates dyslipidaemia and renal function in Zucker obese rats. *J Cell Mol Med* **15**, 1339-1354, doi:10.1111/j.1582-4934.2010.01101.x (2011).

19 Albrecht, T. *et al.* Carnosine Attenuates the Development of both Type 2 Diabetes and Diabetic Nephropathy in BTBR ob/ob Mice. *Sci Rep* **7**, doi:10.1038/srep44492 (2017).
20 Haus, J. M. & Thyfault, J. P. Therapeutic potential of carbonyl-scavenging carnosine derivative in metabolic disorders. *J Clin Invest* **128**, 5198-5200, doi:10.1172/JCI124304 (2018).
21 Matthews, J. J., Turner, M. D., Santos, L., Elliott-Sale, K. J. & Sale, C. Carnosine increases insulin-stimulated glucose uptake and reduces methylglyoxal-modified proteins in type-2 diabetic human skeletal muscle cells. *Amino Acids*, doi:10.1007/s00726-022-03230-9 (2023).
22 Hariharan, R. *et al.* Carnosine supplementation improves glucose control in adults with pre-diabetes and type 2 diabetes: A randomised controlled trial. *Nutr Metab Cardiovasc Dis* **34**, 485-496, doi:10.1016/j.numecd.2023.10.012 (2024).
23 Shoemaker, M. E. *et al.* Differences in muscle energy metabolism and metabolic flexibility between sarcopenic and nonsarcopenic older adults. *J Cachexia Sarcopenia Muscle* **13**, 1224-1237, doi:10.1002/jcsm.12932 (2022).
24 Fabricant, J. D. & Parkening, T. A. Sperm morphology and cytogenetic studies in ageing C57BL/6 mice. *J Reprod Fertil* **66**, 485-489, doi:10.1530/jrf.0.0660485 (1982).
25 Gopko, A. V., Kulibin, A. Y., Semenova, M. L. & Zakhidov, S. T. Carnosine-induced changes in the development of spermatogenic epithelial cells in senescence accelerated SAM mice. *Bull Exp Biol Med* **140**, 235-237, doi:10.1007/s10517-005-0454-4 (2005).
26 Rokicki, J. *et al.* Daily Carnosine and Anserine Supplementation Alters Verbal Episodic Memory and Resting State Network Connectivity in Healthy Elderly Adults. *Front Aging Neurosci* **7**, 219, doi:10.3389/fnagi.2015.00219 (2015).
27 Ding, Q. *et al.* Anserine/Carnosine Supplementation Preserves Blood Flow in the Prefrontal Brain of Elderly People Carrying APOE e4. *Aging Dis* **9**, 334-345, doi:10.14336/AD.2017.0809 (2018).
28 Banerjee, S., Mukherjee, B., Poddar, M. K. & Dunbar, G. L. Carnosine improves aging-induced cognitive impairment and brain regional neurodegeneration in relation to the neuropathological alterations in the secondary structure of amyloid beta (Abeta). *J Neurochem* **158**, 710-723, doi:10.1111/jnc.15357 (2021).
29 Novak, J. C. *et al.* Aging and neuropathic pain. *Brain Research* **833**, 308-310, doi:https://doi.org/10.1016/S0006-8993(99)01522-X (1999).
30 Cho, J. M. *et al.* Late-in-life treadmill training rejuvenates autophagy, protein aggregate clearance, and function in mouse hearts. *Aging Cell* **20**, e13467, doi:10.1111/acel.13467 (2021).
31 Creighton, J. V. *et al.* Physiological Roles of Carnosine in Myocardial Function and Health. *Adv Nutr* **13**, 1914-1929, doi:10.1093/advances/nmac059 (2022).
32 Ririe, D. G., Roberts, P. R., Shouse, M. N. & Zaloga, G. P. Vasodilatory actions of the dietary peptide carnosine. *Nutrition* **16**, 168-172, doi:https://doi.org/10.1016/S0899-9007(99)00268-3 (2000).
33 Takahashi, S., Nakashima, Y. & Toda, K. Carnosine facilitates nitric oxide production in endothelial f-2 cells. *Biol Pharm Bull* **32**, 1836-1839, doi:10.1248/bpb.32.1836 (2009).
34 Weigand, T. *et al.* A Global Cndp1-Knock-Out Selectively Increases Renal Carnosine and Anserine Concentrations in an Age- and Gender-Specific Manner in Mice. *Int J Mol Sci* **21**, doi:10.3390/ijms21144887 (2020).
35 Opurum, P. C. *et al.* Combined sedentarism and high-fat diet induce early signs of kidney injury in C57BL/6J mice. *Am J Physiol Renal Physiol* **328**, F850-F860, doi:10.1152/ajprenal.00259.2024 (2025).
36 Kerr, H. L. *et al.* Mouse sarcopenia model reveals sex- and age-specific differences in phenotypic and molecular characteristics. *J Clin Invest* **134**, doi:10.1172/JCI172890 (2024).

37 Hipkiss, A. R., Preston, J. E., Himswoth, D. T. M., Worthington, V. C. & Abbot, N. J. Protective effects of carnosine against malondialdehyde-induced toxicity towards cultured rat brain endothelial cells. *Neuroscience Letters* **238**, 135-138, doi:10.1016/S0304-3940(97)00873-2 (1997).

38 Wetzel, C. *et al.* Histidine containing dipeptides protect epithelial and endothelial cell barriers from methylglyoxal induced injury. *Sci Rep* **14**, 26640, doi:10.1038/s41598-024-77891-9 (2024).

39 Elbarbary, N. S., Ismail, E. A. R., El-Naggar, A. R., Hamouda, M. H. & El-Hamamsy, M. The effect of 12 weeks carnosine supplementation on renal functional integrity and oxidative stress in pediatric patients with diabetic nephropathy: a randomized placebo-controlled trial. *Pediatr Diabetes* **19**, 470-477, doi:10.1111/pedi.12564 (2018).

40 Jayne, L. *et al.* A torpor-like state in mice slows blood epigenetic aging and prolongs healthspan. *Nat Aging* **5**, 437-449, doi:10.1038/s43587-025-00830-4 (2025).

41 Monroe, T. B. *et al.* Lipid peroxidation products induce carbonyl stress, mitochondrial dysfunction, and cellular senescence in human and murine cells. *Aging Cell*, e14367, doi:10.1111/acel.14367 (2024).

42 Whitsett, J., Picklo, M. J., Sr. & Vasquez-Vivar, J. 4-Hydroxy-2-nonenal increases superoxide anion radical in endothelial cells via stimulated GTP cyclohydrolase proteasomal degradation. *Arterioscler Thromb Vasc Biol* **27**, 2340-2347, doi:10.1161/ATVBAHA.107.153742 (2007).

43 Hu, G. *et al.* Glutathione limits RUNX2 oxidation and degradation to regulate bone formation. *JCI Insight* **8**, doi:10.1172/jci.insight.166888 (2023).

44 Bellantuono, I. *et al.* A toolbox for the longitudinal assessment of healthspan in aging mice. *Nat Protoc* **15**, 540-574, doi:10.1038/s41596-019-0256-1 (2020).

45 Stuart, D. *et al.* Lack of renoprotective effects of targeting the endothelin A receptor and (or) sodium glucose transporter 2 in a mouse model of Type 2 diabetic kidney disease. *Can J Physiol Pharmacol* **100**, 763-771, doi:10.1139/cjpp-2022-0082 (2022).

46 Kittikulsuth, W., Stuart, D., Van Hoek, A. N. & Kohan, D. E. Lack of an effect of nephron-specific deletion of adenylyl cyclase 3 on renal sodium and water excretion or arterial pressure. *Physiol Rep* **3**, doi:10.14814/phy2.12316 (2015).

47 Eshima, H. *et al.* Neutralizing mitochondrial ROS does not rescue muscle atrophy induced by hindlimb unloading in female mice. *J Appl Physiol (1985)* **129**, 124-132, doi:10.1152/japplphysiol.00456.2019 (2020).

48 Shahtout, J. L. *et al.* Inhibition of the skeletal muscle Lands cycle ameliorates weakness induced by physical inactivity. *J Cachexia Sarcopenia Muscle* **15**, 319-330, doi:10.1002/jcsm.13406 (2024).

49 Ferrara, P. J. *et al.* Low lysophosphatidylcholine induces skeletal muscle myopathy that is aggravated by high-fat diet feeding. *FASEB J* **35**, e21867, doi:10.1096/fj.202101104R (2021).

50 Stringer, C., Wang, T., Michaelos, M. & Pachitariu, M. Cellpose: a generalist algorithm for cellular segmentation. *Nat Methods* **18**, 100-106, doi:10.1038/s41592-020-01018-x (2021).

51 Ramkumar, N. *et al.* Loss of Soluble (Pro)renin Receptor Attenuates Angiotensin-II Induced Hypertension and Renal Injury. *Circ Res* **129**, 50-62, doi:10.1161/CIRCRESAHA.120.317532 (2021).

52 Bouxsein, M. L. *et al.* Guidelines for assessment of bone microstructure in rodents using micro-computed tomography. *J Bone Miner Res* **25**, 1468-1486, doi:10.1002/jbmr.141 (2010).

53 Harasymowicz, N. S. *et al.* Intergenerational Transmission of Diet-Induced Obesity, Metabolic Imbalance, and Osteoarthritis in Mice. *Arthritis Rheumatol* **72**, 632-644, doi:10.1002/art.41147 (2020).

1006

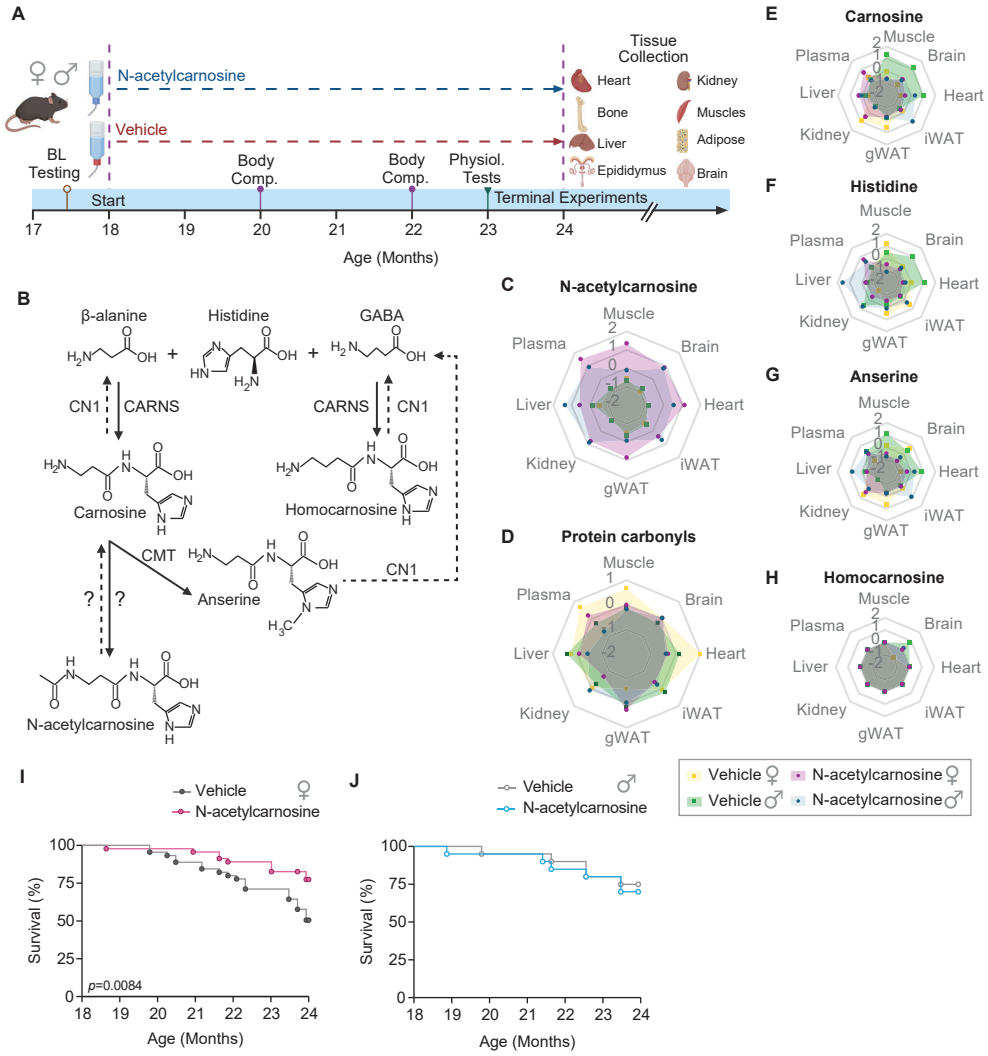
A
N-acetylcarnosine
Vehicle
BL Testing
Start
Body Comp.
Body Comp.
Physiol. Tests
Terminal Experiments
Tissue Collection
Heart
Bone
Liver
Epididymus
Kidney
Muscles
Adipose
Brain
Age (Months)
B
β-alanine
Histidine
GABA
CN1
CARNS
Carnosine
Homocarnosine
CMT
Anserine
N-acetylcarnosine
C
N-acetylcarnosine
D
Protein carbonyls
E
Carnosine
F
Histidine
G
Anserine
H
Homocarnosine
Muscle
Brain
Heart
iWAT
gWAT
Kidney
Liver
Plasma
Vehicle ♀
N-acetylcarnosine ♀
Vehicle ♂
N-acetylcarnosine ♂
I
Survival (%)
p=0.0084
Age (Months)
J
Survival (%)
Age (Months)

Figure 1

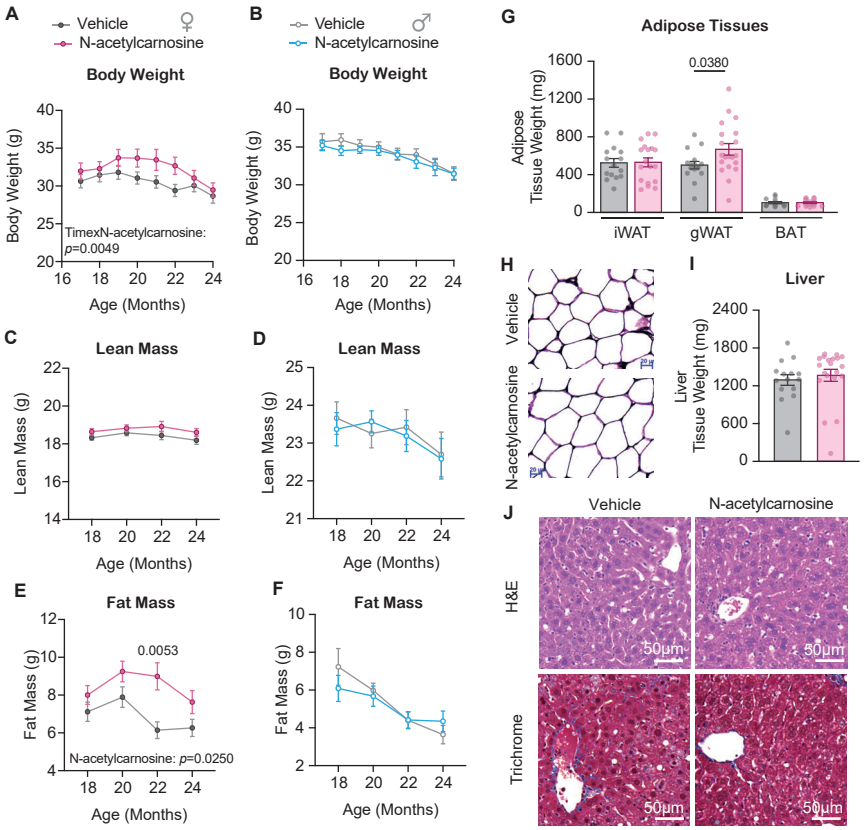
A
Vehicle
N-acetylcarnosine
Body Weight
Body Weight (g)
TimexN-acetylcarnosine: p=0.0049
Age (Months)
B
Vehicle
N-acetylcarnosine
Body Weight
Body Weight (g)
Age (Months)
C
Lean Mass
Lean Mass (g)
Age (Months)
D
Lean Mass
Lean Mass (g)
Age (Months)
E
Fat Mass
Fat Mass (g)
0.0053
N-acetylcarnosine: p=0.0250
Age (Months)
F
Fat Mass
Fat Mass (g)
Age (Months)
G
Adipose Tissues
Adipose Tissue Weight (mg)
0.0380
iWAT
gWAT
BAT
H
Vehicle
N-acetylcarnosine
I
Liver
Liver Tissue Weight (mg)
J
Vehicle
N-acetylcarnosine
H&E
Trichrome
50μm

Figure 2

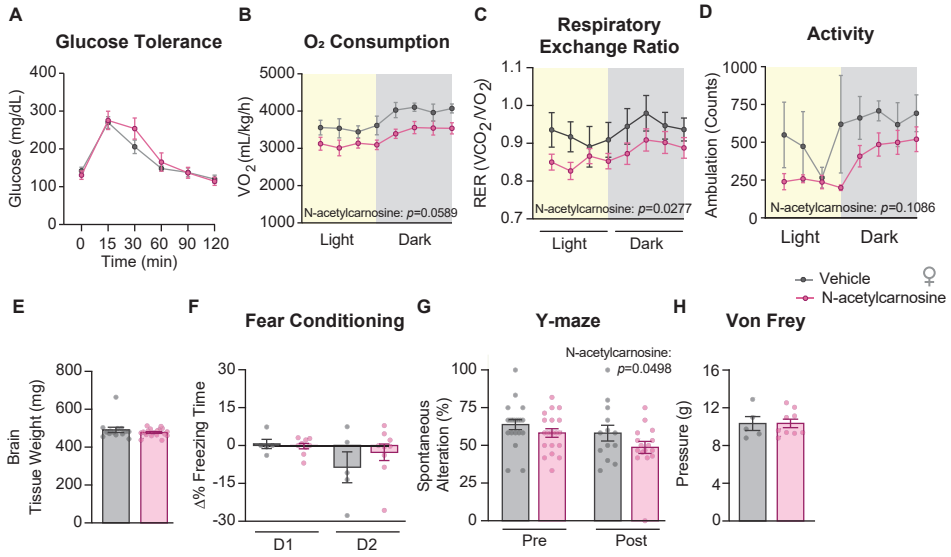
A
Glucose Tolerance
Glucose (mg/dL)
400
300
200
100
0
0 15 30 60 90 120
Time (min)
B
O₂ Consumption
VO2 (mL/kg/h)
5000
4000
3000
2000
1000
N-acetylcarnosine: p=0.0589
Light
Dark
C
Respiratory Exchange Ratio
RER (VCO2/VO2)
1.1
1.0
0.9
0.8
0.7
N-acetylcarnosine: p=0.0277
Light
Dark
D
Activity
Ambulation (Counts)
1000
750
500
250
0
N-acetylcarnosine: p=0.1086
Light
Dark
Vehicle
N-acetylcarnosine
♀
E
Brain Tissue Weight (mg)
800
600
400
200
0
F
Fear Conditioning
Δ% Freezing Time
30
15
0
-15
-30
D1
D2
G
Y-maze
N-acetylcarnosine: p=0.0498
Spontaneous Alteration (%)
100
75
50
25
0
Pre
Post
H
Von Frey
Pressure (g)
16
12
8
4
0

Figure 3

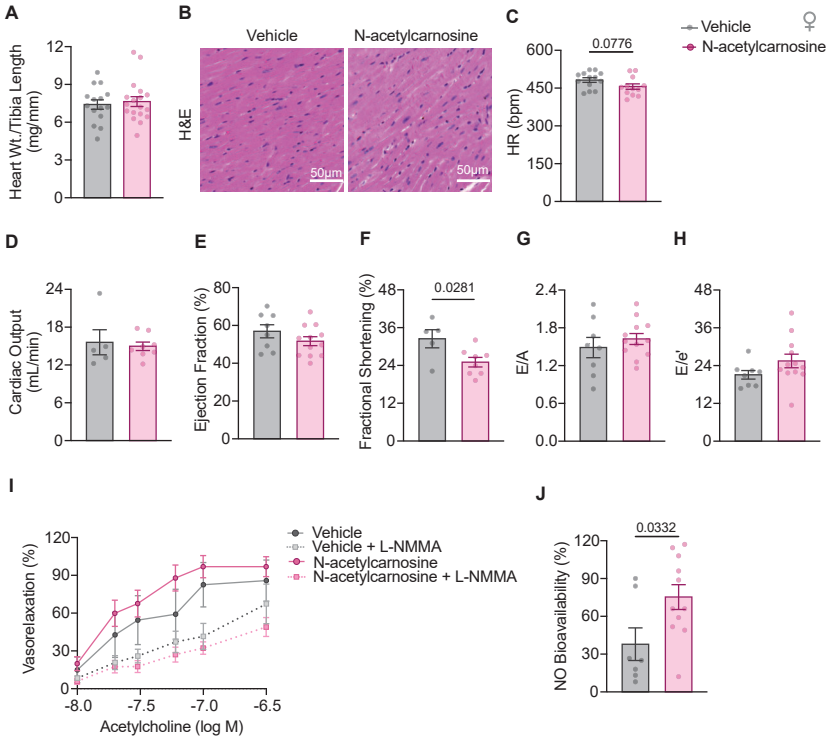
A
Heart Wt./Tibia Length (mg/mm)
B
Vehicle
N-acetylcarnosine
H&E
50μm
50μm
C
HR (bpm)
0.0776
Vehicle
N-acetylcarnosine
♀
D
Cardiac Output (mL/min)
E
Ejection Fraction (%)
F
Fractional Shortening (%)
0.0281
G
E/A
H
E/e'
I
Vasorelaxation (%)
Acetylcholine (log M)
Vehicle
Vehicle + L-NMMA
N-acetylcarnosine
N-acetylcarnosine + L-NMMA
J
NO Bioavailability (%)
0.0332

Figure 4

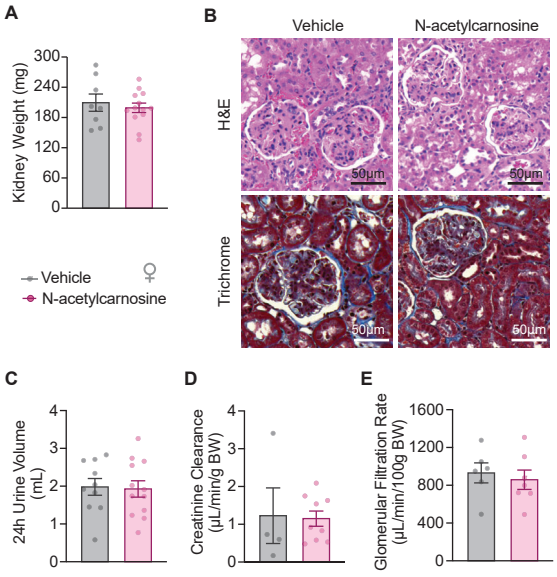
A
Kidney Weight (mg)
300
240
180
120
60
0
Vehicle
N-acetylcarnosine
♀
B
Vehicle
N-acetylcarnosine
H&E
Trichrome
50µm
C
24h Urine Volume (mL)
D
Creatinine Clearance (µL/min/g BW)
E
Glomerular Filtration Rate (µL/min/100g BW)
1600
1200
800
400

Figure 5

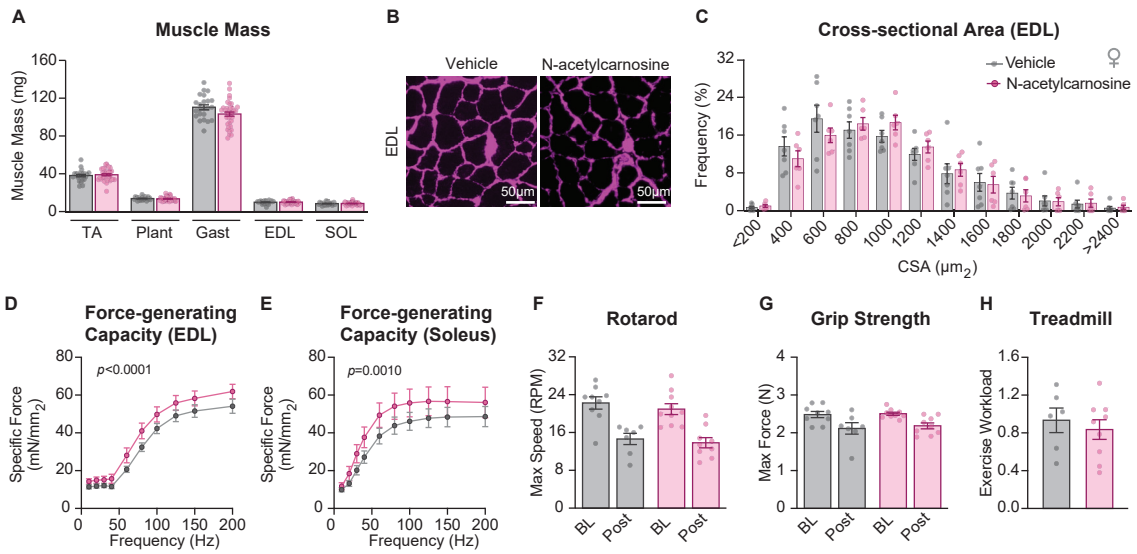
A
Muscle Mass
Muscle Mass (mg)
160
120
80
40
0
TA
Plant
Gast
EDL
SOL
B
Vehicle
N-acetylcarnosine
EDL
50µm
50µm
C
Cross-sectional Area (EDL)
Vehicle
N-acetylcarnosine
Frequency (%)
32
24
16
8
0
<200
400
600
800
1000
1200
1400
1600
1800
2000
2200
>2400
CSA (µm2)
D
Force-generating Capacity (EDL)
p<0.0001
Specific Force (mN/mm2)
80
60
40
20
0
0
50
100
150
200
Frequency (Hz)
E
Force-generating Capacity (Soleus)
p=0.0010
Specific Force (mN/mm2)
80
60
40
20
0
0
50
100
150
200
Frequency (Hz)
F
Rotarod
Max Speed (RPM)
32
24
16
8
0
BL
Post
BL
Post
G
Grip Strength
Max Force (N)
4
3
2
1
0
BL
Post
BL
Post
H
Treadmill
Exercise Workload
1.6
1.2
0.8
0.4
0.0

Figure 6

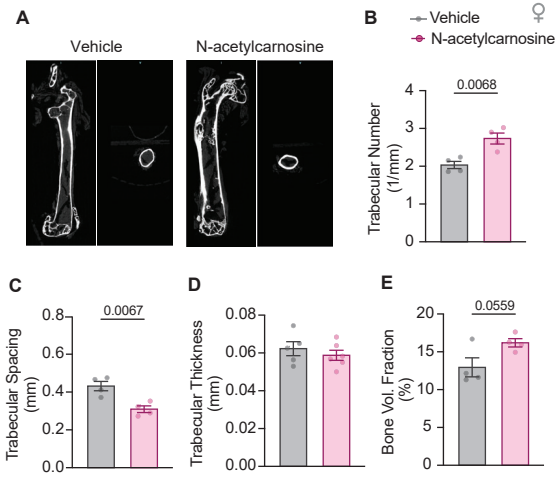
A
Vehicle
N-acetylcarnosine
B
Vehicle
N-acetylcarnosine
♀
0.0068
Trabecular Number (1/mm)
0
1
2
3
4
C
0.0067
Trabecular Spacing (mm)
0.0
0.2
0.4
0.6
0.8
D
Trabecular Thickness (mm)
0.00
0.02
0.04
0.06
0.08
E
0.0559
Bone Vol. Fraction (%)
0
5
10
15
20

Figure 7

		Female		Male		2-Way ANOVA *p*-value		
Tissue	**Metabolite**	**Vehicle**	**N-acetylcarnosine**	**Vehicle**	**N-acetylcarnosine**	**Treatment**	**Sex**	**Sex X Treatment**
Plasma (μM)	N-acetylcarnosine	0.119 (0.038)	81.76 (5.095)	0.051 (0.010)	59.58 (9.438)	**<0.0001**	**0.0408**	**0.0417**
	Carnosine	0.938 (0.149)	1.173 (0.030)	0.816 (0.301)	0.775 (0.145)	0.723	0.353	0.617
	Anserine	1.085 (0.257)	2.292 (1.042)	2.737 (1.028)	2.681(0.134)	0.528	0.274	0.490
	Histidine	38.88 (3.174)	56.95 (8.564)	39.88 (12.48)	52.58 (8.255)	0.194	0.881	0.813
	Homocarnosine	ND	ND	ND	ND	N/A	N/A	N/A
nmol/μg	Protein Carbonyls	5.26 (.457)	4.535 (0.388)	3.790 (0.391)	3.061 (0.957)	0.2425	**0.0242**	0.9964
Urine (μM)	N-acetylcarnosine	29.26 (13.43)	16868 (1384)	1305 (806.2)	15375 (568.1)	**<0.0001**	0.891	0.0945
	Carnosine	23.57 (11.92)	28.95 (8.916)	23.31 (4.175)	34.91 (7.607)	0.343	0.747	0.724
	Anserine	9.948 (3.153)	13.44 (5.114)	35.90 (8.199)	32.15 (5.761)	0.983	**0.0020**	0.554
	Histidine	33.78 (8.553)	50.87 (9.297)	59.02 (10.33)	74.58 (4.587)	0.0728	**0.0112**	0.929
	Homocarnosine	2415 (416.7)	4282 (1373)	3388 (276.4)	3604 (271.6)	0.126	0.821	0.218
Muscle (μmol/kg WW)	N-acetylcarnosine	1.139 (0.726)	8.948 (2.076)	0.718 (0.141)	2.990 (0.424)	**0.0004**	**0.0118**	**0.0253**
	Carnosine	1291 (178.1)	943.8 (137.9)	2133 (57.26)	925.1 (228.1)	**0.0002**	**0.0223**	**0.0177**
	Anserine	4076 (481.3)	3120 (257.8)	5587 (153.5)	2757 (757.1)	**0.0010**	0.243	**0.0650**
	Histidine	394.3 (30.52)	197.7 (24.42)	315.5 (15.12)	124.4 (27.74)	**<0.0001**	**0.0080**	0.914
	Homocarnosine	ND	ND	ND	ND	N/A	N/A	N/A
nmol/μg	Protein Carbonyls	12.16 (3.26)	9.25 (1.35)	9.09 (1.054)	8.76 (0.701)	0.288	0.2436	0.3937
Brain (μmol/kg WW)	N-acetylcarnosine	ND	1.421 (0.154)	0.155 (0.010)	1.373 (0.336)	**<0.0001**	0.776	0.591
	Carnosine	51.74 (6.366)	61.42 (6.131)	81.34 (3.806)	59.800 (3.216)	0.260	**0.0140**	**0.0072**
	Anserine	6.800 (1.494)	3.680 (0.296)	6.220 (0.367)	4.520 (0.495)	**0.0097**	0.876	0.400
	Histidine	61.40 (6.421)	55.64 (4.457)	81.96 (10.94)	58.44 (6.315)	0.0662	0.135	0.249
	Homocarnosine	13417 (1376)	17284 (1766)	20427 (2019)	17889 (412)	0.668	**0.0235**	0.0514
nmol/μg	Protein Carbonyls	18.37 (6.44)	18.32 (3.36)	15.86 (2.47)	18.45 (2.79)	0.774	0.7873	0.766
Heart (μmol/kg WW)	N-acetylcarnosine	ND	6.094 (1.184)	ND	4.264 (0.732)	**<0.0001**	0.207	0.207
	Carnosine	1.776 (0.236)	2.875 (0.649)	7.032 (1.293)	5.172 (1.208)	0.694	**0.0011**	0.139
	Anserine	1.264 (0.134)	2.092 (0.435)	3.939 (0.857)	3.016 (0.478)	0.932	**0.0043**	0.125
	Histidine	56.26 (4.455)	46.26 (1.849)	72.05 (7.118)	49.02 (5.541)	**0.0052**	0.0885	0.221
	Homocarnosine	ND	ND	ND	ND	N/A	N/A	N/A
nmol/μg	Protein Carbonyls	74.51 (38.86)	9.19 (1.12)	34.38 (16.99)	10.18 (1.53)	**0.009**	0.228	0.206
Kidney (μmol/kg WW)	N-acetylcarnosine	0.139 (0.077)	111.2 (13.69)	0.216 (0.104)	117.0 (31.83)	**<0.0001**	0.868	0.871
	Carnosine	6.933 (1.798)	5.227 (1.665)	0.905 (0.066)	1.267 (0.148)	0.592	**0.0009**	0.412
	Anserine	6.059 (0.556)	5.594 (0.599)	2.903 (0.260)	4.907 (1.042)	0.271	**0.0116**	0.0860
	Histidine	21.90 (2.763)	27.01 (2.776)	34.08 (1.292)	35.05 (1.974)	0.203	**0.0004**	0.379
	Homocarnosine	ND	ND	ND	ND	N/A	N/A	N/A
nmol/μg	Protein Carbonyls	9.46 (3.27)	6.63 (1.23)	10.39 (2.45)	11.96 (4.05)	0.8489	0.347	0.507
Liver (μmol/kg WW)	N-acetylcarnosine	0.031 (0.031)	11.798 (1.381)	ND	18.535 (2.937)	**<0.0001**	**0.0318**	**0.0305**
	Carnosine	2.612 (0.293)	2.285 (0.317)	1.355 (0.172)	2.117 (0.360)	0.464	**0.0262**	0.0789
	Anserine	0.745 (0.094)	0.908 (0.149)	1.250 (0.087)	1.289 (0.106)	0.388	**0.0014**	0.592
	Histidine	150.7 (8.947)	155.6 (6.118)	150.2 (5.357)	206.4 (7.287)	**0.0006**	**0.0030**	**0.0025**
	Homocarnosine	ND	ND	ND	ND	N/A	N/A	N/A
nmol/μg	Protein Carbonyls	17.46 (3.87)	15.16 (1.76)	18.66 (5.22)	12.87 (2.78)	0.286	0.882	0.639
iWAT (μmol/kg WW)	N-acetylcarnosine	0.112 (0.022)	14.76 (4.174)	1.747 (0.778)	8.723 (5.318	**0.0037**	0.496	0.242
	Carnosine	29.27 (13.43)	16867 (1385)	1306 (806.2)	15375 (568.1)	**<0.0001**	0.891	0.0945
	Anserine	50.53 (27.89)	19.32 (14.61)	10.08 (5.334)	212.3 (163.0)	0.236	0.289	0.113
	Histidine	22.93 (8.432)	9.142 (1.983)	9.954 (1.329)	19.34 (7.590)	0.700	0.808	0.0568
	Homocarnosine	ND	ND	ND	ND	N/A	N/A	N/A
nmol/μg	Protein Carbonyls	20.26 (3.24)	12.75 (2.87)	17.59 (4.36)	13.85 (3.20)	0.141	0.8313	0.611
gWAT (μmol/kg WW)	N-acetylcarnosine	0.0123 (0.071)	11.669 (7.148)	1.019 (0.446)	3.439 (0.381)	0.0872	0.352	0.250
	Carnosine	5.186 (4.892)	0.393 (0.247)	0.452 (0.054)	0.657 (0.110)	0.393	0.405	0.353
	Anserine	28.05 (25.17)	1.728 (1.119)	1.557 (0.155)	2.439 (0.348)	0.358	0.352	0.327
	Histidine	13.37 (7.114)	4.017 (0.736)	7.105 (0.802)	9.536 (2.703)	0.399	0.927	0.160
	Homocarnosine	ND	ND	ND	ND	N/A	N/A	N/A
nmol/μg	Protein Carbonyls	22.25 (9.83)	33.94 (4.02)	33.16 (12.96)	29.81 (8.42)	0.649	0.712	0.415

Histidine-containing dipeptides and protein carbonyl concentrations across tissues.

Targeted metabolomics via LC-MS was utilized to quantify N-acetylcarnosine, carnosine, anserine, histidine, and homocarnosine in plasma, urine, muscle (TA – HCDs, Gastroc. – carbonyls), brain (cortex), heart (ventricle), kidney, liver, iWAT, and gWAT. Data are presented as Mean ± SEM. Two-way ANOVA was used to test statistical significance. The p-values for the main effects of N-acetylcarnosine treatment (Treatment), sex, and the interaction of these variables (sex x treatment) are reported in the last three columns respectively. Significance was set a $p<0.05$. Bolded p-values indicate a significant main effect.

Supplemental Figure 1

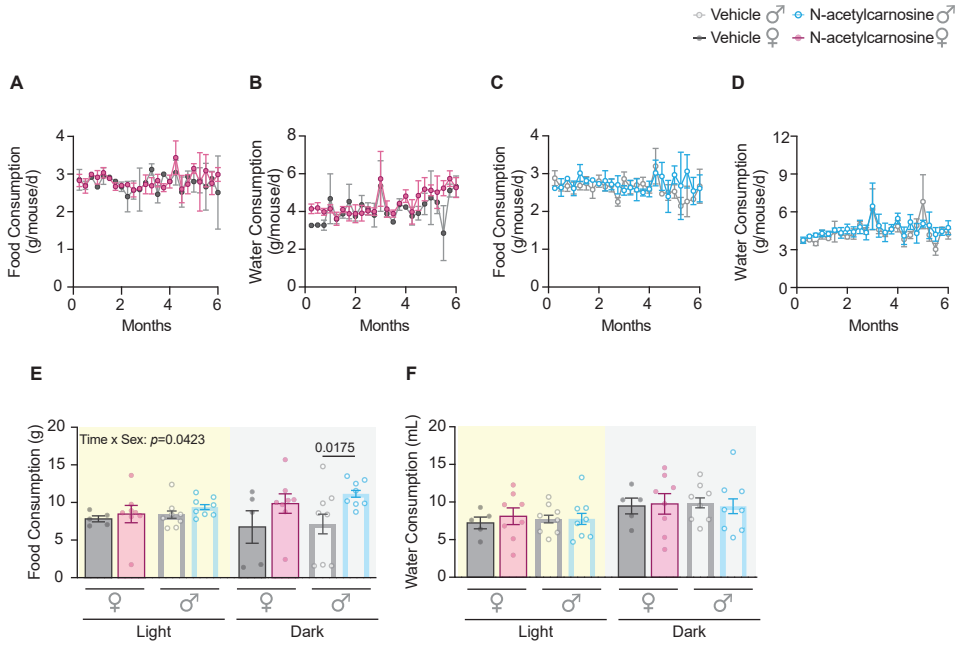

Supplemental Figure 2

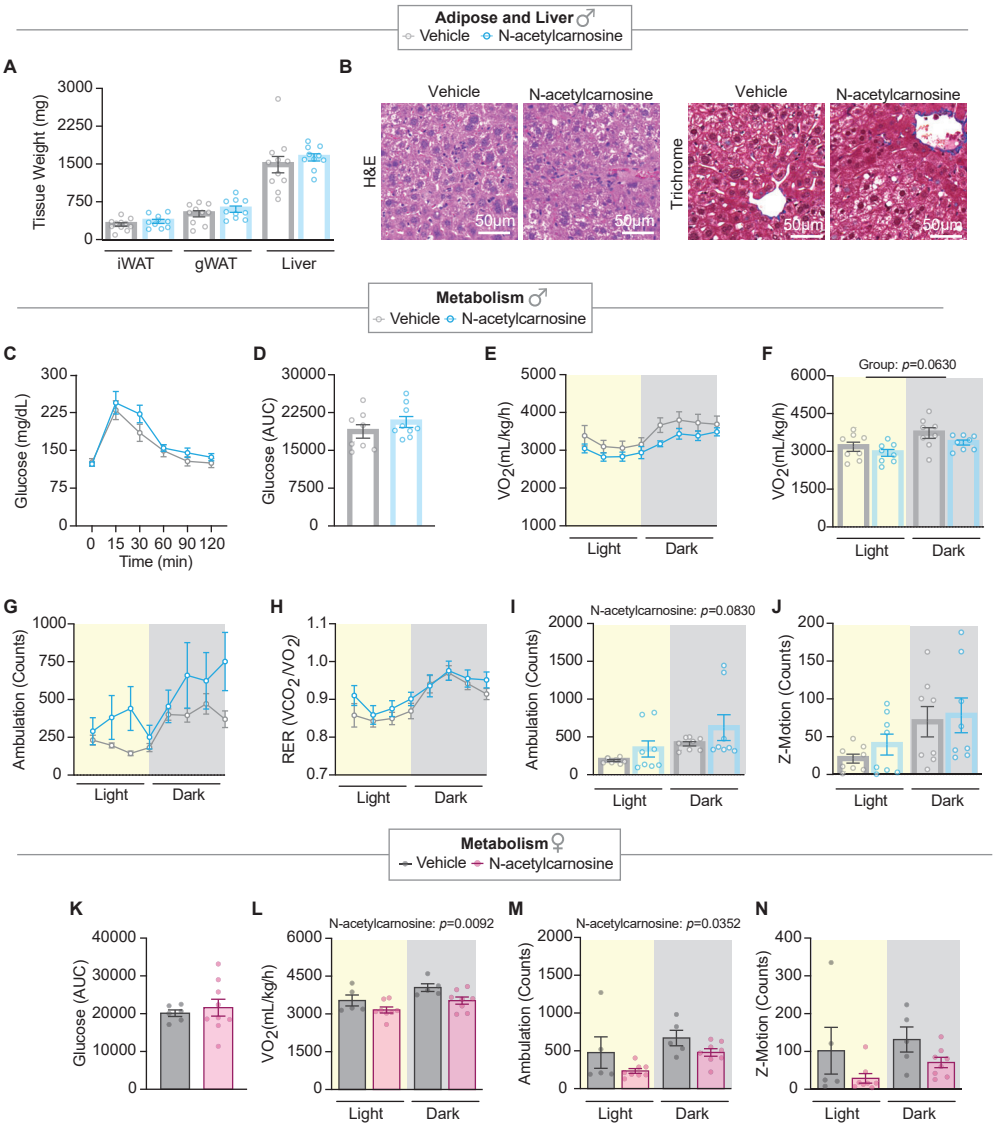

Supplemental Figure 3

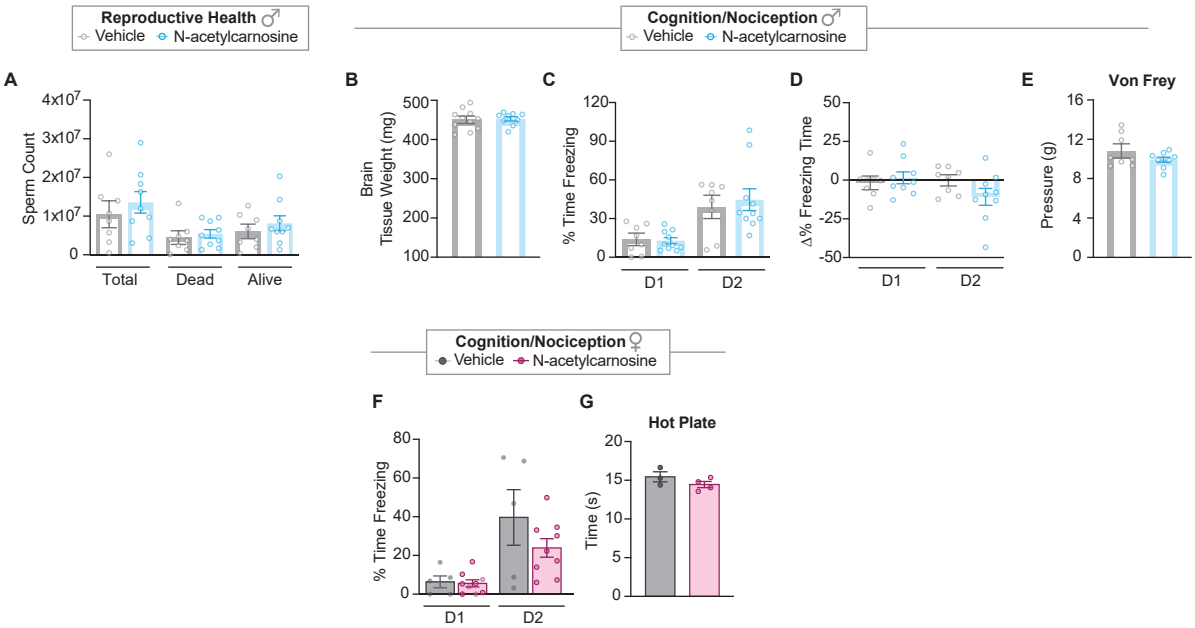

Supplemental Figure 4

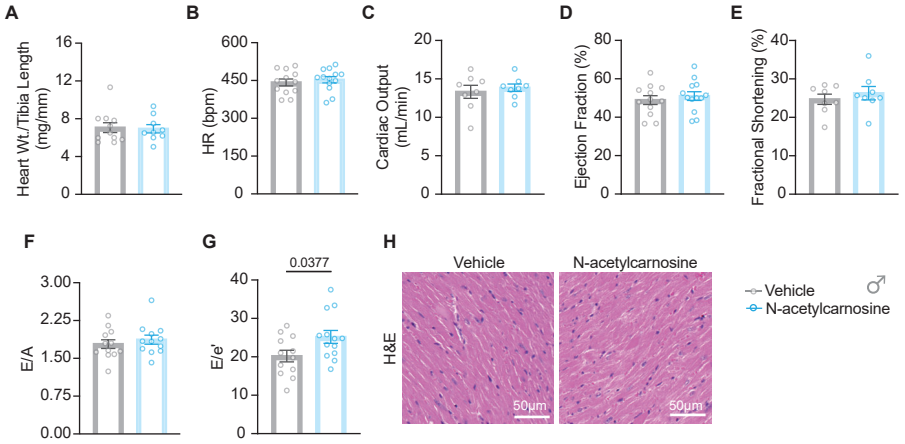

Supplemental Figure 5

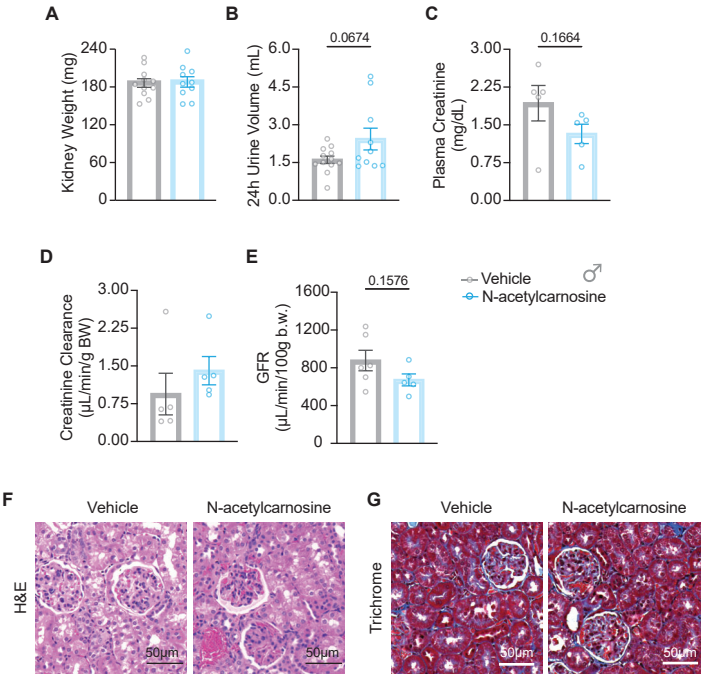

Supplemental Figure 6

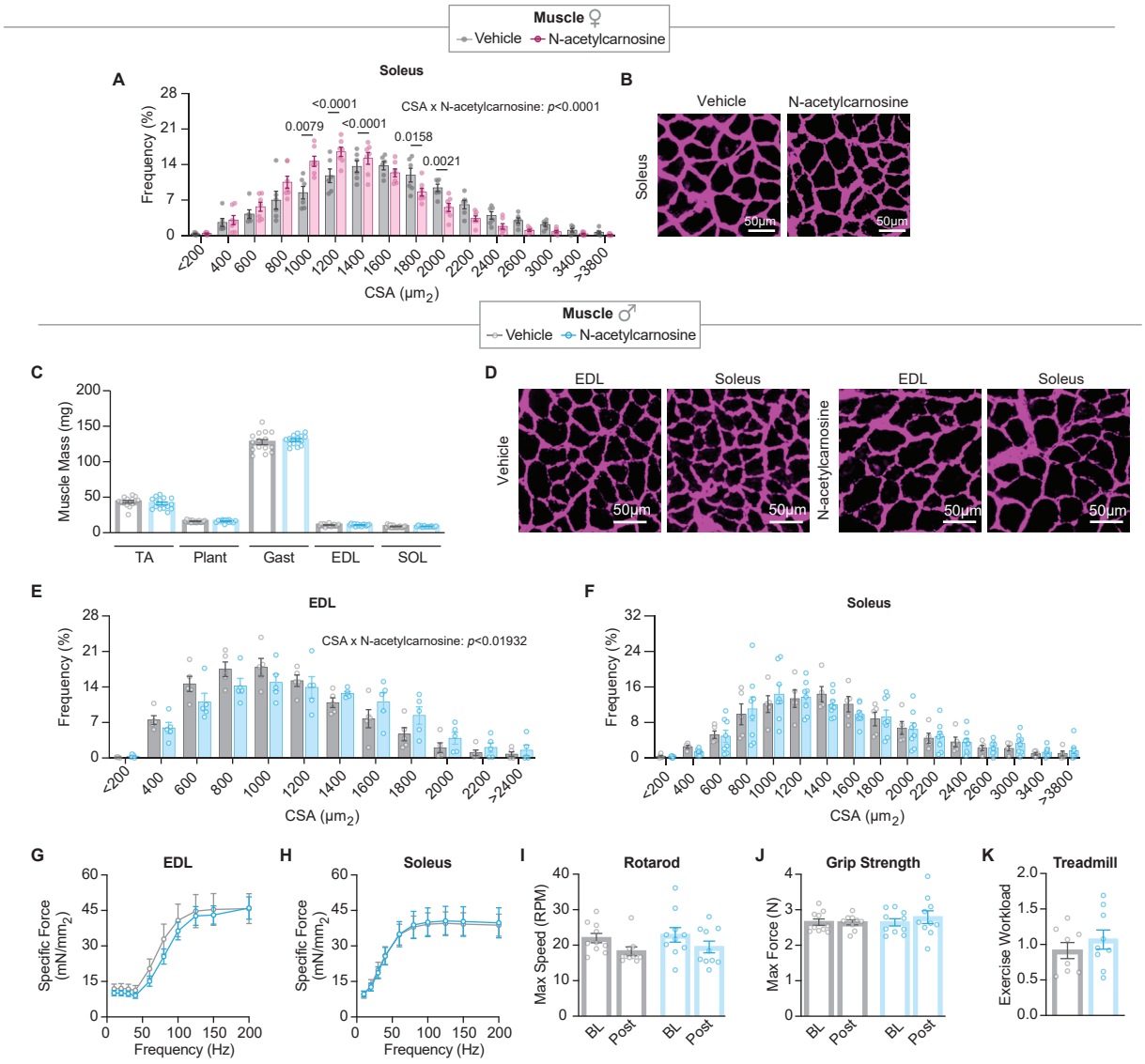

Supplemental Figure 7

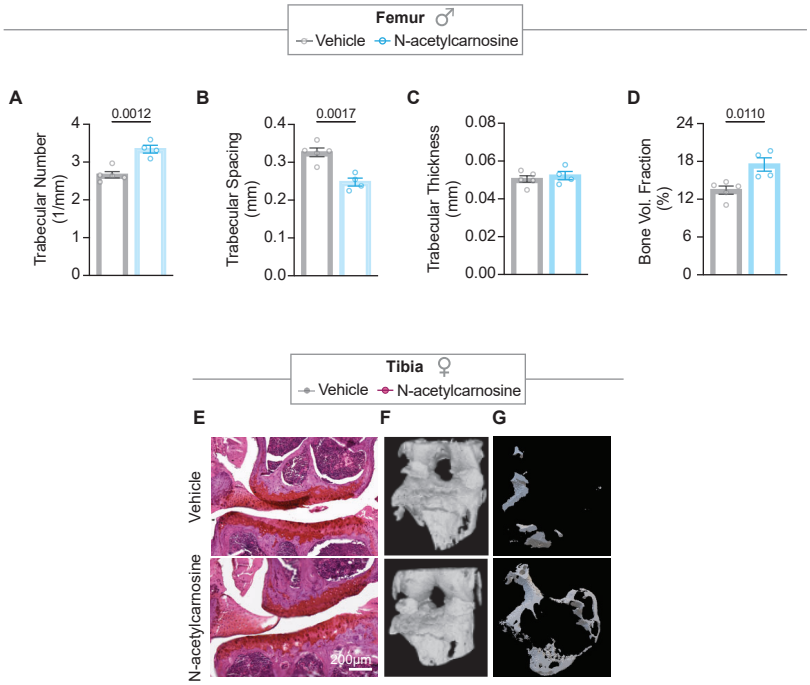

Supplemental Figure 8